Article

Cell Metabolism

The Sense of Smell Impacts Metabolic Health and Obesity

Graphical Abstract

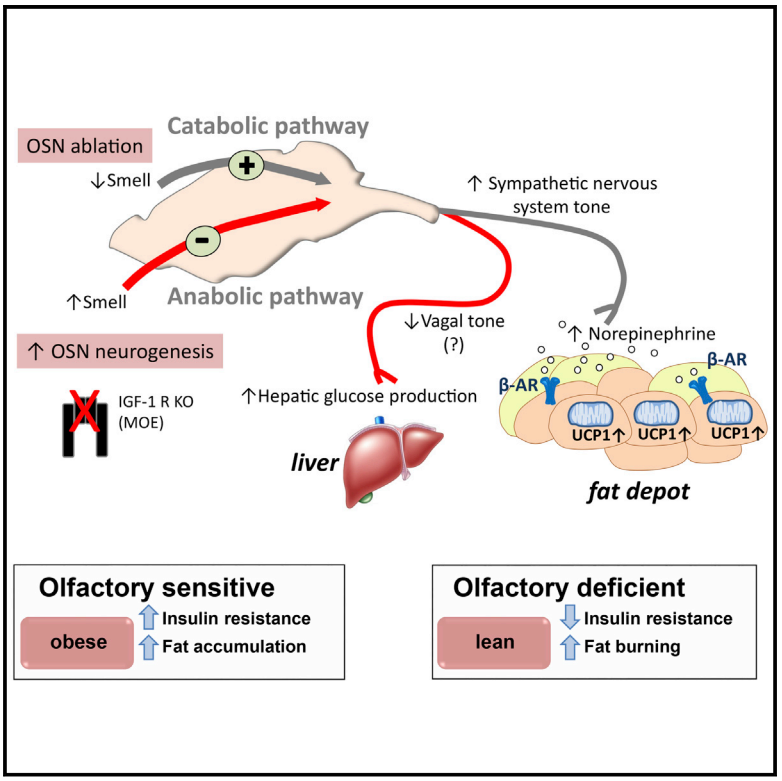

Authors

Celine E. Riera, Eva Tsaousidou, Jonathan Halloran, ..., Andreas Stahl, Jens C. Brüning, Andrew Dillin

Correspondence

bruening@sf.mpg.de (J.C.B.), dillin@berkeley.edu (A.D.)

In Brief

Riera et al. unravel a new bidirectional function for the olfactory system in energy homeostasis. Ablation of olfactory sensory neurons (OSNs) in mice protects them from diet-induced obesity accompanied by increased thermogenesis, while loss of IGF1 signaling in OSNs leads to increased adiposity and insulin resistance.

Highlights

- Loss of adult olfactory neurons protects against diet-induced obesity
- Loss of smell after obesity also reduces fat mass and insulin resistance
- Loss of IGF1 receptors in olfactory sensory neurons (OSNs) improves olfaction
- Loss of IGF1R in OSNs increases adiposity and insulin resistance

Riera et al., 2017, Cell Metabolism *26*, 198–211
July 5, 2017
http://dx.doi.org/10.1016/j.cmet.2017.06.015

CellPress

CellPress

Cell Metabolism
Article

The Sense of Smell Impacts Metabolic Health and Obesity

Celine E. Riera,[1,2,3,10] Eva Tsaousidou,[4,5,6,7,10] Jonathan Halloran,[1,2] Patricia Follett,[8] Oliver Hahn,[6] Mafalda M.A. Pereira,[4,5] Linda Engström Ruud,[4,5] Jens Alber,[4,5] Kevin Tharp,[9] Courtney M. Anderson,[9] Hella Brönneke,[4,5] Brigitte Hampel,[4,5] Carlos Daniel de Magalhaes Filho,[8] Andreas Stahl,[9] Jens C. Brüning,[4,5,6,*] and Andrew Dillin[1,2,11,*]

[1]Howard Hughes Medical Institute and Department of Molecular and Cell Biology
[2]The Paul F. Glenn Center for Aging Research
University of California, Berkeley, Berkeley, CA, USA
[3]Diabetes and Obesity Research Institute, Cedars-Sinai Medical Center, 8700 Beverly Boulevard, Los Angeles, CA, USA
[4]Department of Neuronal Control of Metabolism, Max Planck Institute for Metabolism Research, Gleueler Strasse 50, Cologne, Germany
[5]Center for Endocrinology, Diabetes and Preventive Medicine (CEDP), University Hospital Cologne, Kerpener Strasse 26, Cologne, Germany
[6]Max Planck Institute for Biology of Ageing, Cologne, Germany and Excellence Cluster on Cellular Stress Responses in Aging Associated Diseases (CECAD) Cologne, Germany
[7]Department of Genetics and Complex Diseases and Sabri Ülker Center, Harvard T.H. Chan School of Public Health, Boston, MA, USA
[8]The Salk Institute for Biological Studies, 10010 North Torrey Pines Road, La Jolla, CA, USA
[9]Nutritional Sciences and Toxicology, University of California, Berkeley, Berkeley, CA, USA
[10]These authors contributed equally
[11]Lead Contact
*Correspondence: bruening@sf.mpg.de (J.C.B.), dillin@berkeley.edu (A.D.)
http://dx.doi.org/10.1016/j.cmet.2017.06.015

SUMMARY

Olfactory inputs help coordinate food appreciation and selection, but their role in systemic physiology and energy balance is poorly understood. Here we demonstrate that mice upon conditional ablation of mature olfactory sensory neurons (OSNs) are resistant to diet-induced obesity accompanied by increased thermogenesis in brown and inguinal fat depots. Acute loss of smell perception after obesity onset not only abrogated further weight gain but also improved fat mass and insulin resistance. Reduced olfactory input stimulates sympathetic nerve activity, resulting in activation of β-adrenergic receptors on white and brown adipocytes to promote lipolysis. Conversely, conditional ablation of the IGF1 receptor in OSNs enhances olfactory performance in mice and leads to increased adiposity and insulin resistance. These findings unravel a new bidirectional function for the olfactory system in controlling energy homeostasis in response to sensory and hormonal signals.

INTRODUCTION

The regulation of whole-body energy homeostasis relies on an intricate balance between food intake and energy expenditure. This balance requires the coordinated response of peripheral and central neuronal inputs including hormones, multiple peptides, and neurotransmitters. Notably, these peripheral factors include leptin, insulin, ghrelin, glucagon-like peptide-1 (GLP-1), insulin-like growth factor-1 (IGF1), and cholecystokinin (Belgardt and Brüning, 2010; Clemmons, 2004; Williams and Elmquist, 2012). In order to adapt quickly to variations in environmental conditions and maintain global body homeostasis, mammalian systems have developed neuronal circuits within the central nervous system (CNS) that integrate internal cues into autonomic responses via the sympathetic and parasympathetic nervous systems (Bartness and Song, 2007; Marino et al., 2011). The CNS is responsible for engaging these autonomic systems to control many vital physiological functions, such as pancreatic secretion, lipid storage, thermogenesis, peripheral glucose uptake, and hepatic glucose flux (Marino et al., 2011; Vogt and Brüning, 2013). The variations in autonomic tone are orchestrated by extensive and often reciprocal connections between the hypothalamus and brainstem nuclei (Grill and Hayes, 2012; Skibicka and Grill, 2009; Spencer et al., 1990). In the hypothalamus, the melanocortin system in the arcuate nucleus (ARC) controls feeding in response to circulating insulin and leptin levels (Cowley et al., 2001; Fan et al., 1997; Gropp et al., 2005; Hahn et al., 1998; Huszar et al., 1997; Luquet et al., 2005). Leptin promotes energy expenditure via increasing sympathetic nerve activity and subsequent catecholamine signaling in white adipose tissue (WAT) and brown adipose tissue (BAT), to promote lipolysis and fatty acid oxidation (Bartness and Song, 2007; Collins et al., 1996; Haynes et al., 1997; Lafontan and Langin, 2009; Rahmouni and Morgan, 2007). In addition, cold stimulation or pharmacological activation of the β-adrenergic pathway enhances the formation of brown-like or beige adipocytes predominantly in the inguinal fat pads (iWAT) of rodents, which are characterized by a thermogenic gene expression program similar to that of brown adipose tissue, including high level expression of mitochondrial uncoupling protein 1 (UCP1) (Cousin et al., 1992; Fisher et al., 2012; Petrovic et al., 2010; Seale et al., 2011; Tsukiyama-Kohara et al., 2001; Wu et al., 2012; Young et al., 1984).

Among the many sensory stimuli that influence behavioral decisions about food choice, olfactory inputs are likely to

contribute to the regulation of energy homeostasis. Remarkably, the sensory perception of a hidden food cue, without its ingestion, at least transiently switches the activation state of AgRP and POMC neurons (Betley et al., 2015; Chen et al., 2015). In mice and other rodents, the hypothalamus receives indirect inputs from OSNs through signals entering from the main olfactory bulb (MOB) and transmitted to the centers of the olfactory cortex (Bjorklund et al., 1996; Gascuel et al., 2012). Therefore, olfactory signals may prime the activity of key homeostatic neurons in the hypothalamus to adapt systemic metabolism under conditions of anticipated food intake.

Nutritional status dynamically and profoundly impacts olfactory sensitivity, suggesting the existence of a reciprocal communication between OSNs and the CNS. For example, olfactory acuity is stimulated in the fasted state (Albrecht et al., 2009; Cameron et al., 2012; Soria-Gómez et al., 2014), whereas satiety corresponds to reduced olfactory sensitivity (Critchley and Rolls, 1996). Interestingly, the main olfactory epithelium (MOE) and MOB express high levels of mRNAs for receptors of anorexia-signaling hormones, such as leptin (Ob-R), insulin (IR), and IGF-1, as well as ghrelin receptors (Baskin et al., 1983; Elmquist et al., 1998; Hill et al., 1986). These findings point to the possibility that these hormonal signals not only directly regulate hypothalamic control of peripheral metabolism but might also modulate the sensory perception of the environment via the control of olfaction.

We investigated the role of OSNs in the control of energy balance. To this end, we examined the consequence of genetically ablating the ability of animals to smell, by disrupting OSNs, on whole-body energy homeostasis in lean and obese animals. We find that mice with reduced olfaction, i.e., hyposmia, are leaner upon diet-induced obesity (DIO) either before or after the onset of obesity. These animals exhibit increased energy expenditure and enhanced fat burning capacity as a consequence of enhanced sympathetic nerve activity in BAT and iWAT. Conversely, we describe that conditional ablation of the IGF1 receptor in OSNs results in enhanced olfactory perception. Complementing the results observed in the hyposmic animals, these hyperosmic mice have increased adiposity and insulin resistance. Collectively, the results reveal a critical role for olfactory sensory perception in coordinately regulating peripheral metabolism via control of autonomic innervation.

RESULTS

Genetic Disruption of OSNs Is Associated with Resistance to Diet-Induced Obesity

To explore the possible relationship between olfactory perception and energy homeostasis, we characterized the metabolic consequences of smell disruption in mice. As defects in olfactory perception at birth lead to neonatal lethality in mice (Belluscio et al., 1998; Brunet et al., 1996), we conditionally ablated mature OSNs in adult mice by expressing the inducible diphtheria toxin receptor (DTR) in OSNs using the olfactory marker protein (OMP) promoter (Buch et al., 2005; Buiakova et al., 1996; Chen et al., 2005; Gropp et al., 2005; Li et al., 2004), generating OMP^{DTR} and control animals. OMP labels OSNs from the MOE and the vomeronasal organ (VNO), an organ specialized in pheromone detection to discriminate among gender- and species-specific cues involved in the control of mating and aggressive behavior (Dulac and Torello, 2003). As the DTR transgene of the OMP^{DTR} model is integrated in the genome but only expressed upon Cre-dependent recombination, we further verified the specificity of the OMP promoter by crossing OMP-Cre to a Rosa26 line that expresses tdTomato (RFP) in all Cre-expressing cells (Madisen et al., 2010). Robust RFP detection was detected in OSNs present in the MOE (Figure S1A), the VNO (data not shown), and OSNs axons projecting to the MOB (Figure S1B) but absent in non-olfactory tissues reported to express OMP transcripts such as the thymus, the thyroid, and the bladder (Kang et al., 2015) (Figure S1A). However, weaker OMP expression was detected in discrete cells of the anterior hypothalamus and nerves from the optic chiasm and the cerebellum (Figure S1B). RFP expression overlapped with a polyclonal antibody against OMP in the MOE (Figure S1E), which was not observed in the CNS or non-olfactory tissues.

Ablation of OSNs in OMP^{DTR} mice was induced in 7-week-old animals by diphtheria toxin (DT) injection and validated via assessment of imunoreactive OSNs in the MOE and the VNO using anti-OMP antibodies (Figures 1A and S2A). Such reduction in OSN numbers was not observed upon DT treatment of control animals (*DTR*$^{+/-}$ littermates). OSNs regenerate from stem cell pools which are not OMP positive and have a half-life averaging 4.2 weeks (Chen et al., 2005; Gogos et al., 2000; Margolis et al., 1991), requiring repeated DT-injections every 3 weeks to maintain a state of OSN ablation for chronic studies. Functional olfactory habituation and exploration tests confirmed that OMP^{DTR} mice had a strong impairment in olfactory discrimination of attractive food-based and social odors but still retain some olfactory capacity rendering these animals hyposmic (Figures 1B, S2B, and S2C).

We next assessed whether OSN ablation affected body weight under normal chow diet feeding conditions in lean mice as well as upon induction of DIO upon high-fat-diet feeding. After one DT injection, body weight was reduced in the OMP^{DTR} mice in paired cohorts under normal chow and high-fat diet (HFD), and repeated in an independent experiment (Figures 1C, 1F, and S3A). Strikingly, OMP^{DTR} mice displayed a substantial reduction in body weight (16%) compared to controls upon HFD, as confirmed in an independent cohort (Figures 1F, S3A, and S3B). Food intake was unchanged upon normal chow but was reduced in hyposmic mice upon HFD feeding (Figures 1D, 1E, 1G, and 1H), but without affecting the diurnal feeding pattern (Figure 1I). Importantly, the attenuation of smell did not impact the ability of mice to feed after overnight fasting, and food intake was even enhanced in the first hour of refeeding (Figure S3C). Therefore, the lack of olfactory input leads to a lean phenotype that is not due to a loss of appetite. The reduction of body weight observed in OMP^{DTR} mice reflected a loss in fat mass without alterations in lean mass upon HFD-induced obesity (Figure 1J). In particular, the subcutaneous inguinal fat and the visceral gonadal fat pads were smaller in OMP^{DTR} mice, whereas the composition of other tissues was unaffected (Figure 1K).

Intranasal Ablation of OSNs Slows Weight Gain in DIO Mice

Because Cre recombinase expression is not exclusively restricted to OSNs, we investigated whether the DT injections

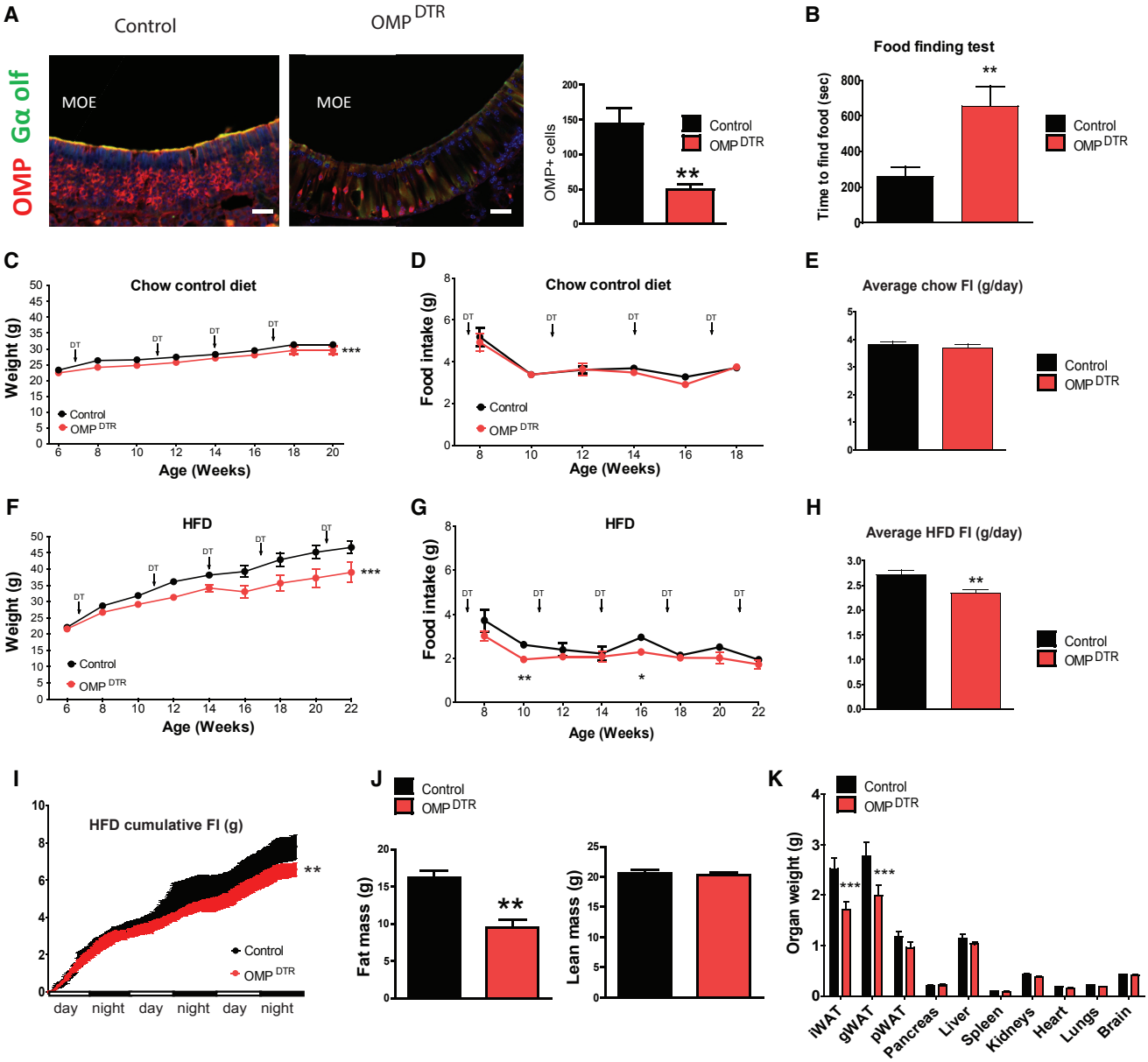

Figure 1. OMP^{DTR} Are Lean and Resistant to Diet-Induced Obesity

(A) DT ablates OMP+ neurons in the MOE of OMP^{DTR}, but not controls, α- OMP (red), Gα olf (green), or dapi (blue). Scale bar, 50 μm. Quantification is in right panel.

(B) Average time needed to find hidden food pellets for random fed mice.

(C–E) Weight gain and weekly and average daily food intake of DT-injected OMP^{DTR} and controls on chow diet (two-way ANOVA for C and D).

(F–H) Weight gain and weekly and average daily food intake of DT-injected OMP^{DTR} and controls when maintained on HFD (two-way ANOVA for F and G).

(I) Feeding pattern of DT-injected OMP^{DTR} and controls on HFD (two-way ANOVA).

(J) Fat mass and lean mass of OMP^{DTR} and controls on HFD.

(K) Body composition of HFD-fed OMP^{DTR} and controls measured by organ weight (g).

Means ± SEM, n = 5–10, ***p < 0.001, **p < 0.001, *p < 0.05.

were causing cellular ablation of certain neuronal subsets in non-olfactory regions. When administered every 3 weeks, DT had very limited effects in brain areas other than OSNs projections into the MOB (Figure S4A) and did not cause abnormal gliosis (Figures S4B and S4C). However, as the DT-mediated cell death model may ablate a few discrete neurons expressing Cre, which could play a role in the lean phenotype observed, we investigated an alternative route to specifically ablate OSNs in the naris. We engineered an adenoviral vector Ad-flex-ta-Casp3-TEVp based on published results of adeno-associated virus (Wu et al., 2014; Yang et al., 2013) for delivery into OMP-Cre animals (OMP-Cre+) and control littermates (OMP-Cre−). Ad-flex-ta-Casp3-TEVp was administered simultaneously with Ad-GFP. Viral delivery was achieved by intranasal injections in order to

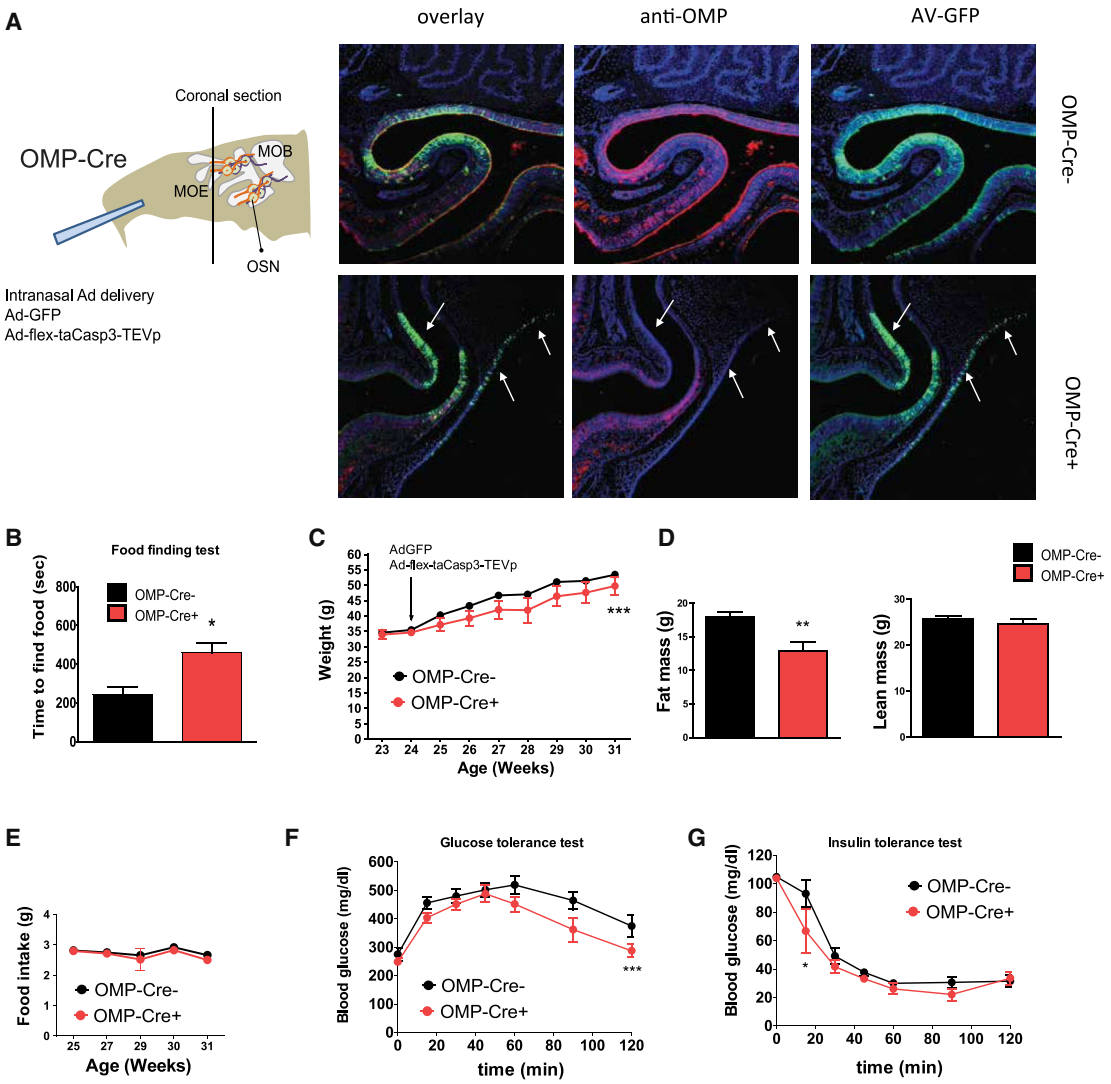

Figure 2. Adenoviral Disruption of OSNs Validates the Lean OMP^{DTR} Phenotype

(A) Strategy to deliver Ad-GFP and Ad-flex-ta-Casp3-TEVp in OMP-Cre− and OMP-Cre+ animals. Ablation of OMP-positive neurons in the MOE of OMP-Cre+ but not controls, α- OMP (red), α- GFP (green), and dapi (blue). Arrows indicate MOE regions where OSNs are depleted.

(B) Average time needed to find hidden food pellets for random fed mice injected with intranasal Ad-GFP and Ad-flex-ta-Casp3-TEVp.

(C–E) (C) Weight gain, (D) fat mass and lean mass, and (E) weekly food intake of Ad-delivered OMP-Cre− and OMP-Cre+ on HFD diet (two-way ANOVA for C and E).

(F and G) Glucose tolerance and insulin tolerance testing of HFD-fed mice after 6 weeks of DIO (two-way ANOVA).

Means ± SEM, n = 5–7, ***p < 0.001, **p < 0.001, *p < 0.05.

robustly target OSNs and increase the expression efficacy (Figure 2A), with no observed penetrance in the MOB or other brain tissues (Figure S4E). OMP-Cre+ mice displayed reduced thickness in the rostral area of the olfactory epithelium and decreased number of OSNs in MOE sections compared to Cre- controls (Figure 2A), and showed reduction in olfactory discrimination compared to controls (Figures 2B, S4D, and S4E). When subjected to DIO, these animals presented reduced body weight and adiposity compared to control mice without differences in lean mass (Figures 2C and 2D). Interestingly, this alternative olfactory depletion method promoted a leaner phenotype than controls without altering food intake (Figure 2E), suggesting that olfactory inhibition leads to reduced obesity, but the degree of hyposmia may impact food intake, as observed in the more complete OMP^{DTR} ablation model (Figure 1). Ad-flex-ta-Casp3-TEVp also ameliorated glucose tolerance in OMP-Cre+ mice (Figure 2F) and provided beneficial effects on insulin sensitivity (Figure 2G). Based on the similarities observed between adenoviral and genetic ablation, these findings suggest that the observed lean phenotype in DIO animals is indeed a specific consequence of reduced olfactory perception.

Hyposmia Is Concomitant to Enhanced Energy Expenditure

From our results, hyposmia results in animals with reduced fat mass despite the ingestion of a high caloric diet. Therefore, the

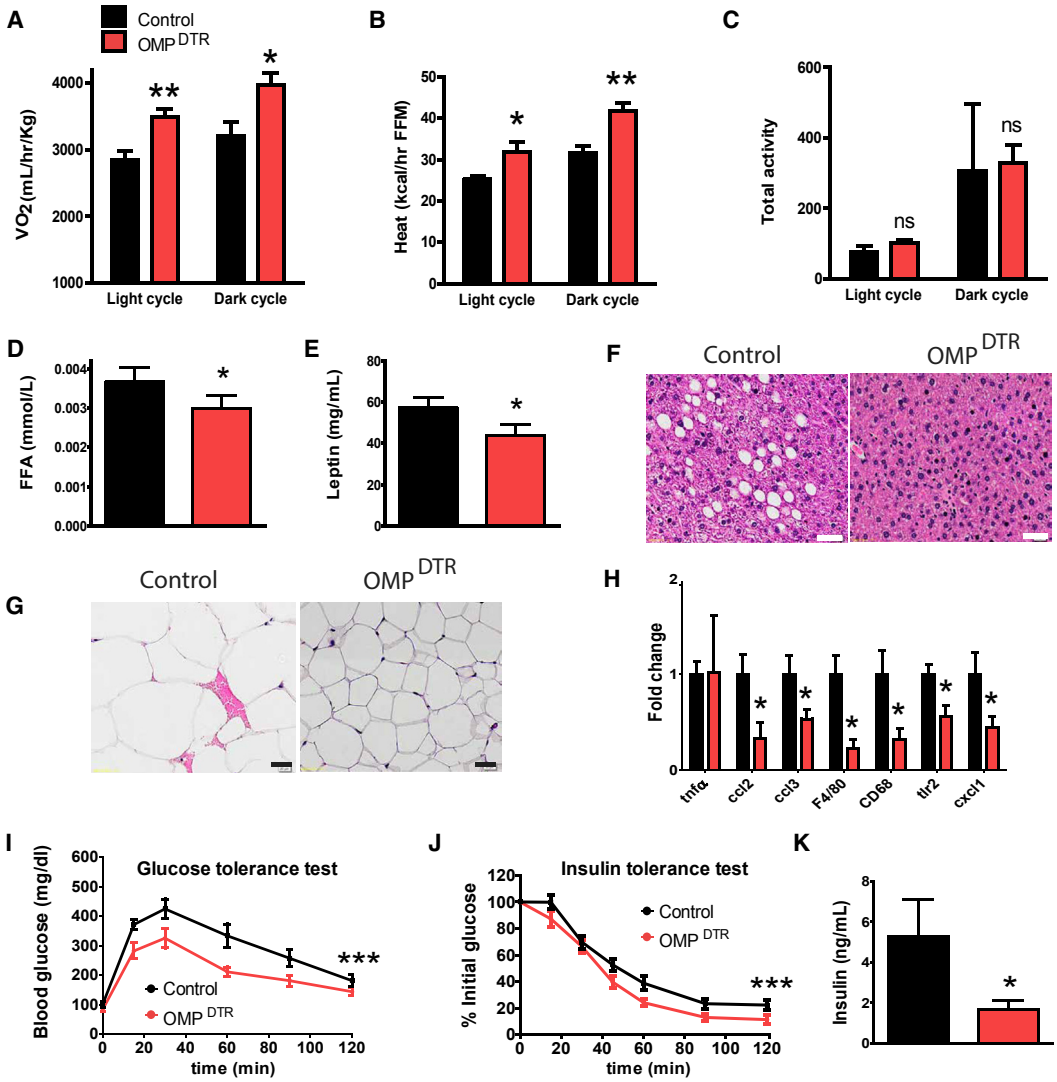

Figure 3. Increased Energy Expenditure in OMP^{DTR}

(A–C) Oxygen consumption, energy expenditure, and total physical activity in HFD-fed DT-injected OMP^{DTR} and control mice measured 2 weeks post DT delivery.
(D and E) (D) Free fatty acid and (E) leptin serum levels.
(F and G) Hematoxylin and eosin sections of liver and gonadal WAT in HFD-fed mice after 14 weeks of DIO. Scale bar, 40 μm.
(H) RTqPCR of pro-inflammatory cytokines and macrophage markers in gonadal WAT from HFD-fed mice after 14 weeks of DIO.
(I and J) Glucose tolerance and insulin tolerance testing of HFD-fed mice after 6 weeks of DIO (two-way ANOVA).
(K) Fasting serum insulin levels.
Means ± SEM, n = 6–11, ***p < 0.001, **p < 0.001, *p < 0.05.

excessive calories are dissipated either in the form of energy utilization or via bodily excretion. To test both hypotheses, we analyzed energy expenditure and energy assimilation in the HFD-fed OMP^{DTR} model. Oxygen consumption and energy expenditure relative to lean body mass were markedly increased in HFD-fed OMP^{DTR} mice compared to controls as measured 2 weeks post DT administration (Figures 3A and 3B). Strikingly, there was no significant difference in physical activity and energy assimilation measured by fecal energy loss between the two genotypes (Figures 3C and S3D), indicating that the reduced weight gain was mainly due to combined effects of increased energy expenditure and a reduction in food intake in HFD-fed OMP^{DTR} mice (Figures 3B and 1D), but not due to differences in nutrient absorption. Furthermore, OMP^{DTR} mice had decreased circulating free fatty acids and fasting leptin levels (Figures 3D and 3E) and were protected against pathological phenotypes typical of the effects of HFD feeding after 14 weeks of HFD treatment, such as hepatic steatosis (Figure 3F) and visceral adipocyte hypertrophy (Figure 3G).

The development of insulin resistance due to DIO is mediated in part by chronic inflammation in adipose tissue characterized by the recruitment of macrophages and elevation of chemokine expression in fat (Lumeng et al., 2007; Xu et al., 2003a). Accumulation of macrophage infiltrates was visible by hematoxylin and eosin staining in visceral fat depots of control mice under DIO but was far less abundant in OMP^{DTR} mice after 14 weeks of

DIO (Figure 3G). Similarly, HFD feeding induced expression of markers of inflammation in visceral fat tissue but was largely attenuated in OMP^{DTR} mice (Figure 3H). Consistent with decreased inflammation, OMP^{DTR} mice had improved insulin sensitivity, improved glucose tolerance, and lower fasting insulin levels after 6 weeks of DIO (Figures 3I–3K). Taken together, hyposmia is associated with protection against many of the negative features caused by excessive caloric intake.

Disrupted Olfaction Is Linked to Adipose Tissue Thermogenesis and Browning of Subcutaneous Fat

Because hyposmic mice were protected from the severity of excessive caloric intake, we began to ask how these animals were equilibrating the intake of calories with their peripheral metabolism. BAT dissipates energy directly as heat through uncoupling fatty acid oxidation from ATP production by increasing UCP1 within mitochondria (Enerbäck et al., 1997). While control animals on prolonged HFD feeding showed lipid accumulation in BAT, OMP^{DTR} mice exhibited healthy histological features of BAT despite prolonged HFD feeding (Figure 4A). After 14 weeks of DIO, the brown fat of hyposmic mice had a striking reduction in the number of fat vacuoles (Figure 4A) expected for a higher thermogenic capacity. Additionally, OMP^{DTR} mice had elevated expression for many genes involved in mitochondrial biogenesis and genes enriched in BAT, including Ucp1, Ucp2, Cox5b, CytC, and Pgc1α (Figure 4B). Concordantly, BAT fat pads from OMP^{DTR} mice had increased mitochondrial respiration (Figure 4C). In line with increased thermogenic capacity leading to increased fatty acid oxidation, increased expression of genes is involved in fatty acid oxidative metabolism from adipose tissue of OMP^{DTR} mice (Figure 4D).

Increased thermogenesis and browning of fat can be profoundly modulated by inputs from the sympathetic nervous system through the release of catecholamine (Bartness and Song, 2007; Cousin et al., 1992; Haynes et al., 1997; Young et al., 1984). We found a drastic increase in circulating levels of the catecholamine noradrenaline, a major agonist of β-adrenergic receptors, in OMP^{DTR} mice consistent with increased thermogenesis in fat (Figure 4E). Transcript levels of the β-adrenergic receptor Adrb3, a critical mediator of fat thermogenesis and lipolysis, was substantially elevated in BAT and iWAT from OMP^{DTR} mice (Figure 4F). Prolonged β-adrenergic receptor activity induces the emergence of brown-like adipocytes in subcutaneous iWAT which display thermogenic properties and contribute to energy dissipation (Petrovic et al., 2010). Strikingly, iWAT isolated from OMP^{DTR} mice had large pockets of cells with the multilocular morphology characteristic of brown-like adipocytes (Figure 4G). Consistent with fat browning of white adipose tissue, a thermogenic program was strongly activated in iWAT from OMP^{DTR} mice. Levels of Ucp1 mRNA-expression were upregulated by 40-fold, and levels of Cidea were also increased (Figure 4H).

Excessive calories stored in fat can be utilized by the activation of lipases capable of converting the large lipid stores into usable triglycerides. One such enzyme, hormone-sensitive lipase (HSL), hydrolyzes intracellular triacylglycerol and diacylglycerol and is one of the key enzymes controlling lipolysis. Triggering β-adrenergic receptors promotes lipolysis through a cAMP cascade leading to PKA-mediated phosphorylation and activation of HSL (Carmen and Víctor, 2006). We found that the total levels of HSL were similar among genotypes; however, levels of activated, phosphorylated (Ser 660) HSL were increased in WAT from OMP^{DTR} mice (Figures 4I and S4E), pointing toward enhanced lipid catabolism in the hyposmic mice. Consistent with activation of HSL, the isoproterenol-induced lipolysis rate was increased in OMP^{DTR} mice compared to control adipocytes (Figure 4J), whereas unstimulated lipolysis was similar among genotypes (Figure S3F), confirming increased stimulation of β-adrenergic signaling in adipose depots of the hyposmic animals. In addition, OMP^{DTR} mice presented a lower respiratory quotient compared to controls (Figure S3G) as a response to increased fatty acid oxidative metabolism. Altogether, these results demonstrate that the lean phenotype observed in OMP^{DTR} mice is due to increased sympathetic nerve activity resulting in increased fat thermogenesis.

Hyposmia Attenuates Further Weight Gain upon High-Fat Feeding

The results presented thus far indicate that hyposmia can mitigate DIO in mice prior to being placed on a high caloric diet. To explore the possibility that loss of olfaction could also mitigate DIO of mice already obese due to increased caloric intake, we ablated OSNs in DIO glucose-intolerant mice. We found that one single injection of DT was sufficient to reduce adiposity in the severely obese animals, and repeated injections maintained reduced body weight and fat mass despite continued HFD feeding of these mice (Figures 5A, 5B, and S5A). This strong reduction in fat mass, but not lean mass, was achieved without reducing food intake (Figure 5C) and was mediated by increased energy expenditure (Figure 5F). As observed in animals in which OSNs were ablated prior to DIO, these mice had improved glucose clearance (Figure 5D), insulin sensitivity (Figure S5B), increased oxygen consumption, and lower basal insulin levels (Figures S5C and S5D).

Elevated leptin levels observed in obesity and type 2 diabetes mellitus contribute to impaired hypothalamic leptin signaling, thus leading to leptin's failure to suppress appetite and promote energy expenditure (Balthasar et al., 2004; Cowley et al., 2001). To examine leptin action in OMP^{DTR} mice, we performed a leptin sensitivity test prior and post DT injection. The anorectic effects of leptin were detectable in both control and OMP^{DTR} mice before DT injection (Figure 5E). DT administration enhanced leptin's ability to lower food intake in the OMP^{DTR} animals compared to controls. Additionally, DT-injected OMP^{DTR} animals also presented improved energy expenditure upon leptin treatment compared to controls and untreated OMP^{DTR} mice (Figure 5F), suggesting that the reduction of olfactory inputs in mice increased leptin sensitivity upon overnutrition.

Loss of IGF1 Receptor in the Olfactory Epithelium Promotes Increased Olfactory Sensitivity

Since our results indicated that reducing olfactory sensitivity is associated with improved metabolic fitness, we investigated whether the converse manipulation of olfactory acuity would worsen metabolic health. In line with this hypothesis, the potassium-dependent Na^+/Ca^{2+} exchanger Nckx4 mutant mice present reduced body weight and impaired olfactory acuity (Stephan et al., 2011), whereas diabetic mice lacking leptin (*ob/ob*) or

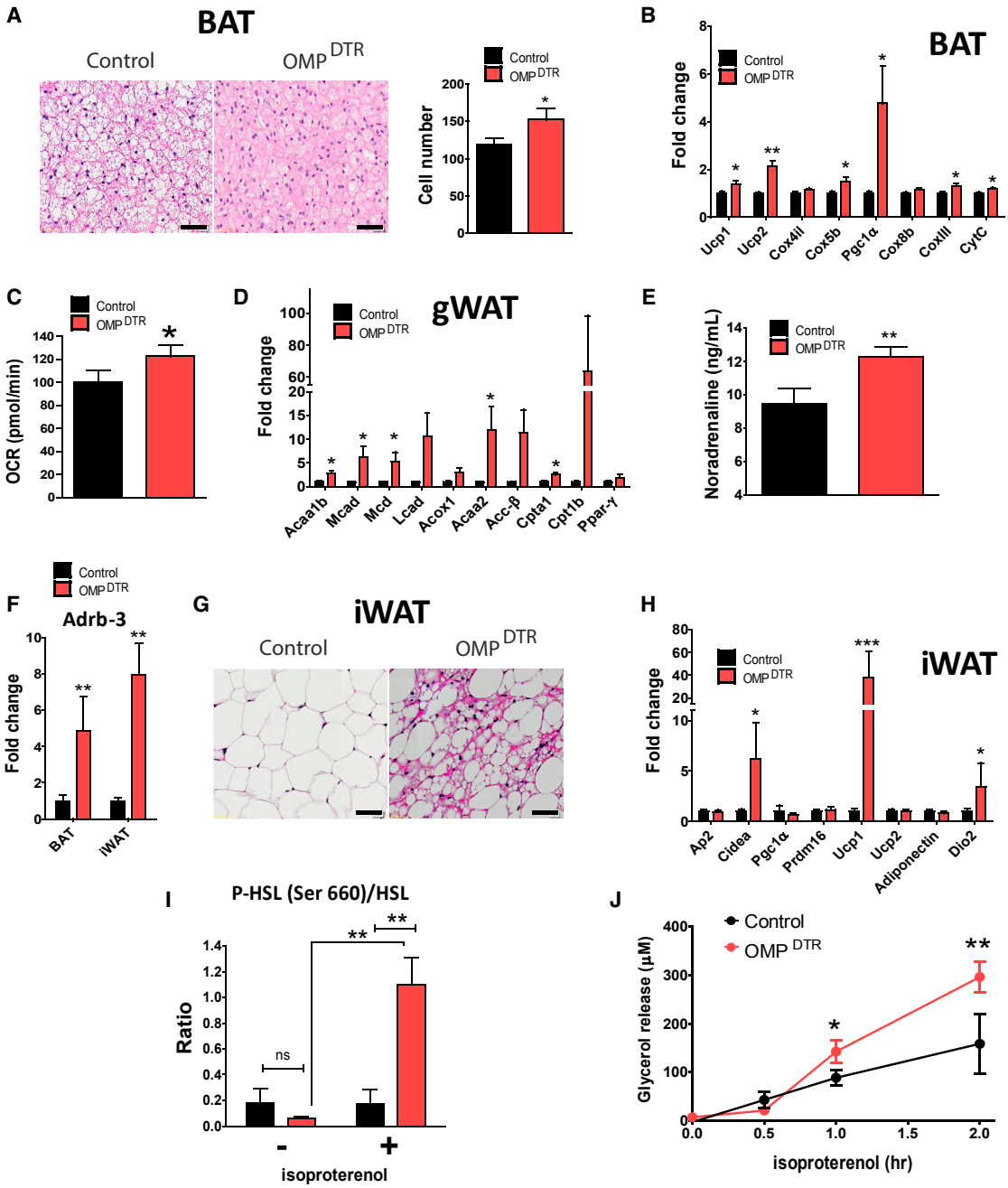

Figure 4. OMP^{DTR} Have Increased Thermogenesis in Adipose Tissue

(A) Hematoxylin and eosin staining of brown fat depots and brown adipocytes number in HFD-fed OMP^{DTR} and controls. Right panel, n = 3, cells counted on a section of 300 μm^2. Scale bar, 50 μm.

(B) RTqPCR of mitochondrial genes in brown fat of HFD-fed OMP^{DTR} and control mice.

(C) OCR of BAT from HFD-fed OMP^{DTR} and control littermates analyzed by Seahorse extracellular flux analyzer after 14 weeks of DIO.

(D) RTqPCR against fatty acid oxidation genes in gonadal fat of HFD-fed OMP^{DTR} and control littermates after 14 weeks of DIO.

(E) Noradrenaline serum levels after 14 weeks of DIO.

(F) Adrb-3 gene expression levels (RTqPCR) in brown and inguinal fat depots after 14 weeks of DIO.

(G) Presence of multilocular adipocytes in the inguinal fat depots by hematoxylin and eosin staining after 14 weeks of DIO. Scale bar, 50 μm.

(H) RTqPCR against brown fat and thermogenic genes in inguinal fat of HFD-fed OMP^{DTR} and control mice after 14 weeks of DIO.

(I) Phospho (Ser 660) HSL levels normalized to total HSL in WAT from HFD-fed OMP^{DTR} and controls after isoproterenol or saline injection after 14 weeks of DIO.

(J) Lipolysis rates in adipocytes exposed to isoproterenol from gonadal WAT isolated from HFD-fed OMP^{DTR} and control mice after 14 weeks of DIO.

Means ± SEM, n = 3–12, ***p < 0.001, **p < 0.001, *p < 0.05.

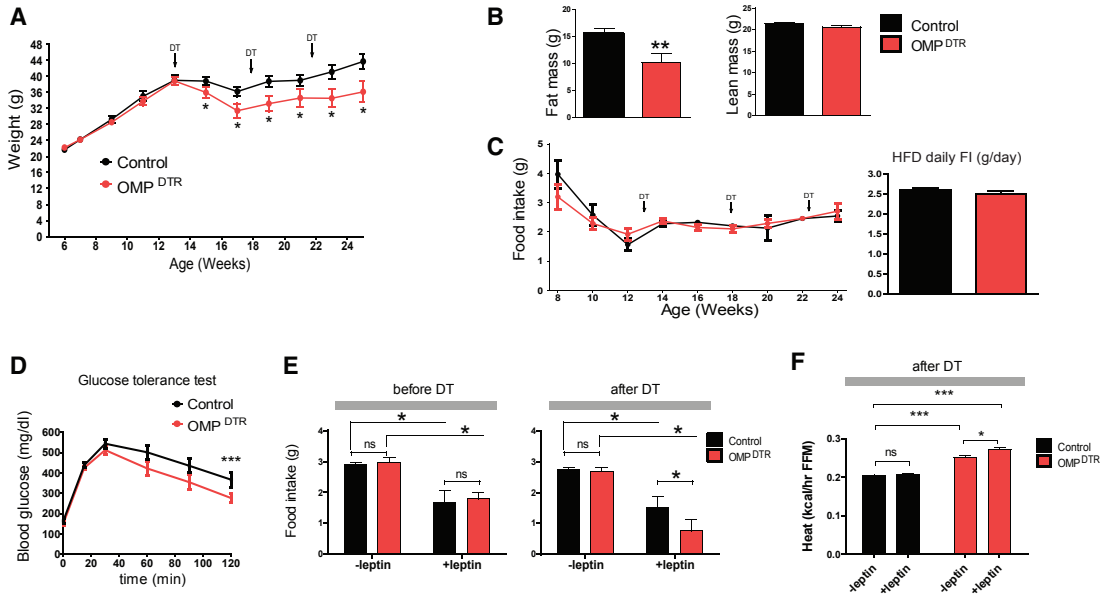

Figure 5. Olfactory Inhibition Restores Metabolic Health in Obese Animals

(A) Weight gain and adiposity of HFD-fed OMP^{DTR} and controls before and after DT injection after 7 weeks of DIO.

(B) Fat mass and lean mass of OMP^{DTR} and controls.

(C) Weekly food intake in DT-injected OMP^{DTR} and controls.

(D) Glucose tolerance test of HFD-fed mice (two-way ANOVA).

(E and F) Daily food intake and energy expenditure in a subgroup of OMP^{DTR} and control littermates before and after leptin administration 2 weeks after DT delivery.

Means ± SEM, n = 4–10, ***p < 0.001, **p < 0.001, *p < 0.05.

leptin receptors (*db/db*) can locate food ten times faster than wild-type, and this effect can be abrogated in *ob/ob* mice by daily leptin injections (Getchell et al., 2006). As the olfactory bulb contains a high density of insulin receptors (Hill et al., 1986), leptin receptors (Shioda et al., 1998), and other endocrine hormone receptors (Palouzier-Paulignan et al., 2012), we considered that hormonal inputs might be able to adjust olfactory perception. Additionally, insulin application in the olfactory mucosa has been shown to regulate odorant-evoked electroolfactogram responses, suggesting that olfactory control depends on nutritional status (Lacroix et al., 2008). IGF1 has previously been established as a factor influencing peripheral regeneration of OSNs *in vitro* and *in vivo* (Pixley et al., 1998), and IGF1R ablation in NSCs is responsible for enhanced neurogenesis in the olfactory bulb and improved olfactory function (Chaker et al., 2015). Based on this knowledge, we thought to create a new model of loss of IGF1 receptors (IGF1Rs) in the MOE as a complementary genetic tool to the OMP^{DTR} model to manipulate olfactory perception and study its impact on metabolic function.

In situ hybridization confirmed the presence of IGF1R in the MOE (Figure S6A). We then explored the consequence of impairing IGF1R expression in MOE. Mice homozygous for the loxP-flanked IGF1R allele (IGF1R$^{flox/flox}$) were crossed with OMP-Cre animals to generate IGF1R$^{\Delta OMP}$ mice. As expected, these animals had reduced abundance of IGF-1R mRNA specifically in OSNs as determined by RNAscope (Figure S6A) and reduced transcript levels as measured by RT-qPCR and RNAsequencing on isolated olfactory epithelium (Figure S6B). We also verified that mutation of IGF1R in the MOE did not affect levels of IR as revealed by RT-qPCR analysis and RNAsequencing on isolated olfactory epithelium (Figure S6C). Moreover, global comparative gene expression analysis on olfactory epithelium of control and IGF1R$^{\Delta OMP}$-mice revealed 2,123 significantly differentially regulated genes ($p \leq 0.05$) between both genotypes (Figure S6D). Interestingly, this mRNA-expression analysis revealed a differential regulation of genes associated with OSN maturity, with a higher expression of genes characteristic for immature OSNs in IGF1R$^{\Delta OMP}$ mice, whereas expression of markers of mature OSNs were significantly decreased in these mice compared to controls (Figure S6D). One-sided Fisher's exact test confirmed a significant enrichment for immature markers in the set of upregulated genes and mature markers in the set of downregulated genes with a p value less than $1e^{-20}$ in both cases, whereas the enrichment for immature marker genes in the downregulated set and mature marker genes in the upregulated set was not significant (p values of 0.98 and 1, respectively, Figure S6D).

To further validate the differential regulation of markers of immature and mature OSNs in the absence of OSN-intrinsic IGF-1 signaling, we assessed the mRNA expression of several immature and mature markers (Figure S6E). This analysis revealed an enrichment in growth-associated protein 43 (GAP43), a canonical marker for immature OSNs (McIntyre et al., 2010), and nescient helix loop helix 2 (Nhlh2), a factor involved in neuronal development (Nickell et al., 2012). Surprisingly, previously identified markers of mature OSNs were reduced in IGF1R$^{\Delta OMP}$ mice (Figure S6E). In line with the mRNA abundance profile of MOE tissue, immunostaining of

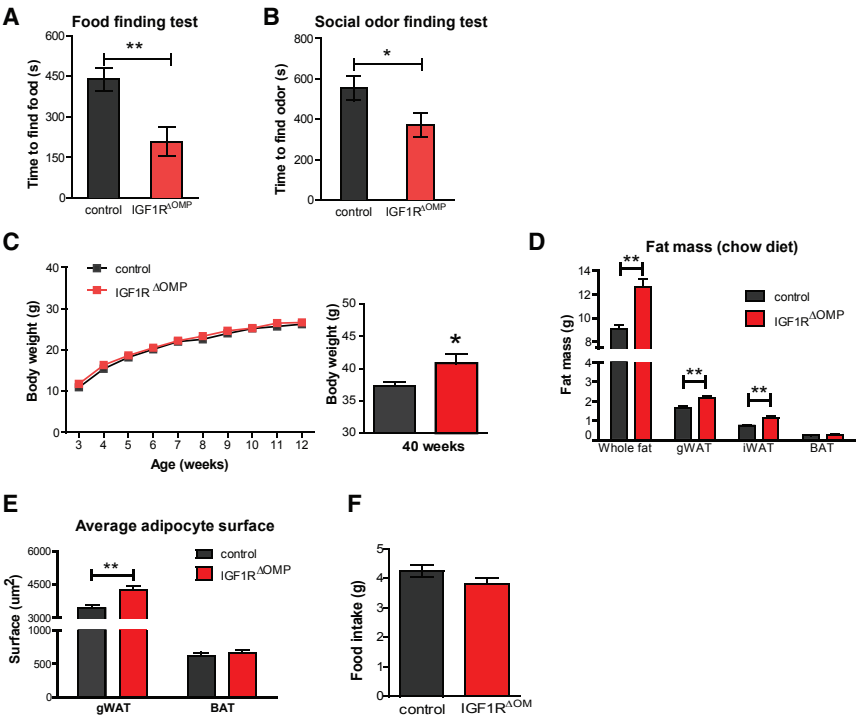

Figure 6. IGF1R Ablation in the Olfactory Epithelium Results in Obesity upon Chow Control Diet

(A) Average time needed to find hidden food pellets for random fed mice.

(B) Average time needed to find a hidden Q-tip immersed in female urine for random fed mice.

(C) Growth curve of control and IGF1R $^{\Delta OMP}$ mice on chow diet, 3–12 weeks (left panel) and 40 weeks (right panel).

(D) Fat mass of control and IGF1R $^{\Delta OMP}$ mice at 40 weeks.

(E) Average adipocyte surface quantification of gonadal WAT and BAT of control and IGF1R$^{\Delta OMP}$ mice at 40 weeks.

(F) Average daily food intake of control and IGF1R$^{\Delta OMP}$ mice at 15 weeks.

Means ± SEM, n = 5–16, ***p < 0.001, **p < 0.001, *p < 0.05.

GAP43 revealed a higher abundance of this protein in MOE section (Figures S7A and S7B), whereas Kcnq2 was reduced (Figures S7C and S7D). These data suggest that the MOE of IGF1R$^{\Delta OMP}$ mice undergoes increased proliferation of immature cells that could potentially result in reduced mature OSNs. To address whether mature cells were under-represented, we quantified the average number of OMP-positive neurons in td-Tomato $^{\Delta OMP}$ mice and found it to be unaffected by this MOE remodeling (Figures S7B and S7D). Additionally, RT-qPCR revealed no significant changes in the markers of apoptosis caspase-3 and -4 but a significant increase in mKi67 expression, demonstrating an increased proliferation in the olfactory epithelium of IGF1R$^{\Delta OMP}$ mice (Figure S6E).

Interestingly, MOE remodeling upon loss of IGF1R functionally translated into an improved olfactory performance in IGF1R$^{\Delta OMP}$ mice, as evidenced by an increased ability in locating a food source and increased reactivity in locating a social odor (Figures 6A and 6B) without any impairment in odor discrimination and detection as measured by an olfactory habituation and dishabituation test (Figure S6F). Taken together, these findings indicate that loss of IGF1 receptors in the MOE promotes an increased proliferation of immature OSNs resulting in hyperosmia of these mice.

Increased Adiposity in IGF1R$^{\Delta OMP}$ Mice

To define the physiological consequences of reducing IGF1R expression in OSNs, remodeling MOE, and improving olfactory performance, we assessed adiposity and body weight in IGF1R$^{\Delta OMP}$ mice compared to control mice. Upon normal chow diet feeding, these mice presented a body weight comparable to controls until 12 weeks; however, further analysis revealed a significant, age-dependent weight gain in these animals (Figure 6C). This increased body weight was accompanied by excessive adipose tissue mass in the gonadal and inguinal fat depots (Figure 6D). Particularly, the gonadal fat pad had enlarged adipocytes compared to control animals (Figure 6E), accompanied by non-significant reduction in energy expenditure, oxygen consumption, and respiratory quotient (Figures S7E–S7G). Importantly, adipose expansion was independent of food intake, which remained unchanged compared to controls (Figure 6F). Globally, markers of browning and particularly Dio2 (Figure S7H) were reduced in the subcutaneous inguinal fat pads of these animals, and Ucp1 expression was reduced in gWAT (Figure S7I), whereas these markers were unaffected in brown fat (Figure S7J). Taken together, these findings indicate that inhibition of IGF1 signaling in OSNs enhances olfactory perception and in turn promotes adiposity.

Insulin Resistance and Reduced Suppression of Hepatic Glucose Production Are Associated with Improved Olfactory Capacity

To assess the regulation of peripheral glucose metabolism of IGF1R$^{\Delta OMP}$ and control mice, we performed insulin and glucose tolerance tests in these animals (Figures 7A and 7B). IGF1R$^{\Delta OMP}$ mice exhibited impaired insulin sensitivity compared to controls, while glucose tolerance was unaffected. To further investigate which aspect of peripheral glucose metabolism was differentially modulated, we performed euglycemic-hyperinsulinemic clamp studies comparing IGF1R$^{\Delta OMP}$ and control animals. While both groups achieved the same degree of glycemia during the steady-state phase of the clamp (Figure 6D) and exhibited similar degree of glucose disappearance (Figures 7D and 7F), the glucose infusion rate (GIR) required to maintain euglycemia was significantly reduced in IGF1R$^{\Delta OMP}$ mice (Figures 7C and 7E).

When we assessed hepatic glucose production (HGP), IGF1R$^{\Delta OMP}$ and control mice exhibited no significant differences in baseline, but IGF1R$^{\Delta OMP}$ mice exhibited a reduced ability of insulin to suppress HGP (Figure 7G). However, insulin's ability to

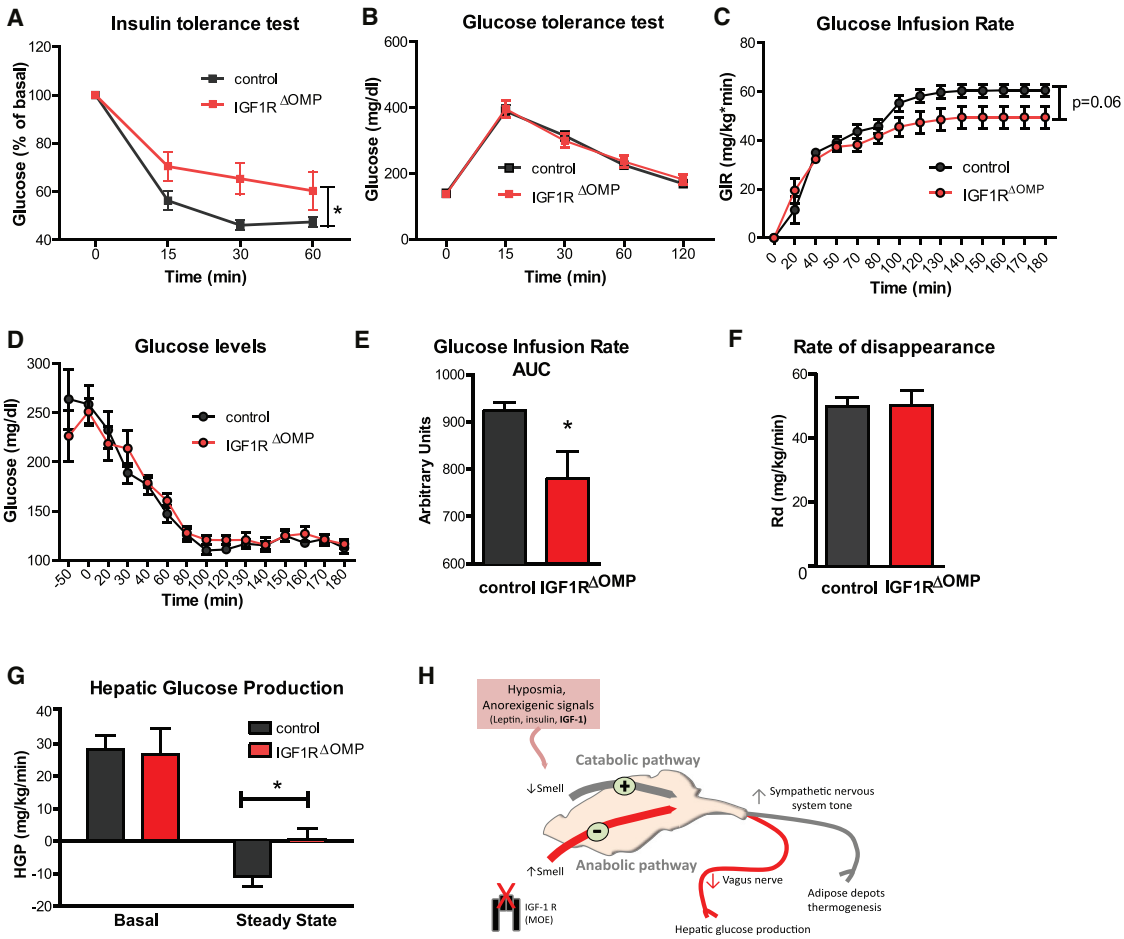

Figure 7. IGF1R Ablation in OSNs Promotes Insulin Resistance and Impaired Insulin-Induced Suppression of Hepatic Glucose Production

(A and B) Insulin and glucose tolerance tests of control and IGF1R$^{\Delta OMP}$ mice at 11 and 12 weeks, two-way ANOVA test.

(C and D) Glucose infusion rate and glucose levels during a hyperinsulinemic-euglycemic CLAMP of control and IGF1R$^{\Delta OMP}$ mice at 22 weeks.

(E) Area under curve of the glucose infusion rate (CLAMP).

(F) Rate of disappearance (CLAMP).

(G) Hepatic glucose production at basal and steady state (CLAMP).

(H) Model for the regulation of energy balance by olfactory neurons.

Means ± SEM, n = 8–16, ***p < 0.001, **p < 0.001, *p < 0.05.

promote glucose uptake into peripheral tissues including brown fat, gonadal fat, skeletal muscle, and the brain remained unaltered (Figure S8H). Importantly, IGF1R$^{\Delta OMP}$ mice were hyperinsulinemic and hyperleptinemic in random fed conditions compared to the control mice (Figure S8I). Thus, inhibition of IGF1R in OSNs promotes peripheral insulin resistance and pinpoints the ability of OSNs to influence autonomic control of hepatic glucose production.

DISCUSSION

Since the discovery of hypothalamic circuits influencing anabolic and catabolic processes, very little information has been gathered on the role of sensory inputs in the regulation of energy homeostasis pathways. We establish that OSNs actively participate in the modulation of peripheral metabolism in response to external and internal cues. Prior to our work, multiple studies have demonstrated that the initiation and cessation of feeding behaviors are associated with changes in olfactory sensitivity. Hunger arouses olfactory perception (Albrecht et al., 2009; Cameron et al., 2012; Soria-Gómez et al., 2014), whereas a dampening of olfactory sensitivity is observed after the ingestion of a meal and therefore correlates with a satiety signal (Savigner et al., 2009). Thus, given the existing precedents linking olfaction with feeding behavior, we characterized in depth the consequence of either impairing or improving olfaction on metabolic homeostasis.

We discovered that reduced olfactory inputs initiate prolonged sympathetic responses to severe energy depletion through increased β-adrenergic signaling in adipose tissue, therefore promoting increased lipolysis in gonadal fat and increased thermogenesis in brown and subcutaneous fat fads. In humans, hyposmia is commonly accompanied by the loss of flavor from food, with subsequent loss of appetite and weight loss or

anorexia (Bonfils et al., 2005; Henkin and Smith, 1971). We observe an adipose mass decrease in our study without overt food aversion (Figures 5B and 5C). Thus, our data support the notion that reduced olfactory output triggers a metabolic response mimicking the cessation of feeding and thus leads to catabolic energy utilization needed to protect animals from a high caloric diet (Figure 7H).

In our second mouse model, we demonstrate that loss of IGF1R in the olfactory epithelium confers opposing effects to the ablation of OSNs, and increases smell perception (Figures 6D and 6E). Notably, these mice displayed increased adiposity accompanied by hyperleptinemia, hyperinsulinemia, and insulin resistance (Figures 7A and S7L). Strikingly, insulin's ability to suppress HGP is impaired in these animals, pointing to a new role for IGF1 in OSNs in the control of peripheral insulin resistance (Figure 7G). IGF1, which shares 48% amino acid identity with proinsulin, has been implicated in ameliorating insulin sensitivity in both rodent models and human subjects (Clemmons, 2004), and suppression of liver IGF1 promotes hyperinsulinemia and insulin resistance by acting on skeletal muscle (Fernández et al., 2001; Yakar et al., 2001). The data presented here support a more complex model in which IGF1 also functions in OSNs to regulate peripheral insulin sensitivity. In addition, how OSNs signal this information to the liver remains to be determined. One plausible explanation implicates OSN communication with the CNS. Indeed, central insulin action in the CNS is necessary for the suppression of endogenous glucose production. In particular, AgRP-expressing neurons play a critical role in the suppression of HGP by the regulation of vagal efferent nerves in the liver (Könner et al., 2007; Obici et al., 2002; Pocai et al., 2005). Our results suggest that OSNs also contribute to the regulation of HGP and could function upstream of ARC neurons.

Despite the link that we observe between OSNs, energy expenditure, and adiposity, we cannot fully exclude that unspecific manipulation of non-olfactory CNS neurons expressing OMP-Cre may also affect the observed weight phenotypes (Figures S1C and S1D). Nevertheless, intranasal delivery of the Ad-flex-ta-Casp3-TEVp adenovirus selectively reduced OSNs without CNS penetrance and reproduced the metabolic benefits of the genetic ablation model, although to a lesser extent associated with the weaker ablation of OSNs using this method (Figure 2). Consistent with our findings, a mouse model with reduced smell, the Nckx4 mutant mouse, presents reduced body weight and impaired olfactory acuity (Stephan et al., 2011), whereas a hyperosmic phenotype is observed in diabetic mice lacking leptin (*ob/ob*) or leptin receptors (*db/db*)(Getchell et al., 2006). Nonetheless, our hypothesis is challenged by the whole-body deletion of the voltage-gated K(+) channel (Kv) subtype Kv1.3 channel, a mouse model of enhanced olfactory sensitivity (Tucker et al., 2012) which shows resistance to DIO (Tucker et al., 2012; Xu et al., 2003b). The exact contribution of the olfactory system in this particular model remains to be determined, as Kv1.3 is highly expressed throughout the brain and non-neuronal tissues, including liver and skeletal muscle (Xu et al., 2003b). Therefore, whether the lean phenotype of the hyperosmic Kv1.3 knockout animals comes from their enhanced smell acuity or from other sites of action remains unclear.

The finding that OSNs can control peripheral metabolism is intriguing, and multiple mechanisms could be engaged in this circuitry. It is mainly thought that the hypothalamus receives indirect inputs from OSNs through the MOB and transmitted to the centers of the olfactory cortex (Purves et al., 2001; Su et al., 2009). Interestingly, direct connections between discrete subpopulations of OSNs and several nuclei from the hypothalamus, such as the paraventricular nucleus (PVN), the supraoptic nucleus (SO), and the luteinizing hormone-releasing hormone (LHRH)-secreting neurons, have been observed (Bader et al., 2012; Yoon et al., 2005), reinforcing the idea that an active circuitry initiated in OSNs might influence metabolic homeostasis. Our data strongly indicate a circuit that relays information to autonomic neurons and may require central neurons, including hypothalamic pro-opiomelanocortin (Pomc) neurons in the arcuate nucleus of the hypothalamus which exert their anorexigenic effects by activating melanocortin-4 receptors and an autonomic response (Cowley et al., 2001; Wardlaw, 2011). In line with this hypothesis, fiber photometry recording of AgRP and POMC neurons activity in the hypothalamus of awake, behaving animals shows that the perception of food rapidly switches the activation state of these neurons upon hunger and can be immediately reversed by removing the food cues (Chen et al., 2015). Additionally, olfactory inputs may be integrated by a complex interplay of different hypothalamic and brainstem nuclei expressing appetite-modulatory neuropeptides. Regardless, the potential of modulating olfactory signals in the context of the metabolic syndrome or diabetes is attractive. The data presented here show that even relatively short-term loss of smell improves metabolic health and weight loss, despite the negative consequences of being on a HFD.

STAR★METHODS

Detailed methods are provided in the online version of this paper and include the following:

- KEY RESOURCES TABLE
- CONTACT FOR REAGENT AND RESOURCE SHARING
- METHOD DETAILS
  - Animal Care
  - Genetic mouse models
  - Indirect Calorimetry, Physical Activity, and Food Intake
  - Food finding test
  - Social odor finding test
  - Habituation-dishabituation test
  - Metabolic studies
  - Ex vivo lipolysis
  - Protein analysis
  - Leptin sensitivity
  - Quantitative PCR analysis
  - Adenovirus propagation and titration
  - Immunofluorescence and histological studies
  - Hyperinsulinemic-euglycemic CLAMPS
  - Adipose tissue oxygen consumption
  - Bomb fecal calorimetry
  - RNA sequencing
  - RNAscope analysis
  - Data and Software Availability
  - Statistical methods

SUPPLEMENTAL INFORMATION

Supplemental Information includes seven figures and one table and can be found with this article at http://dx.doi.org/10.1016/j.cmet.2017.06.015.

AUTHOR CONTRIBUTIONS

C.E.R. executed most of the olfactory ablation experiments, and E.T. characterized the IGF1R$^{\Delta OMP}$ model. C.E.R., E.T., A.D., and J.C.B. planned the majority of the experiments and wrote the manuscript. J.H. and P.F. performed animal husbandry maintenance and assistance to metabolic studies. O.H. performed bioinformatic analyses of the RNaseq data. M.M.A.P., L.E.R., and B.H. assisted E.T. during tissue analysis experiments. J.A. and H.B. assisted with the setup of behavioral experiments. K.T., C.M.A., and C.D.M.F. assisted CE.R. .during tissue analysis experiments.

ACKNOWLEDGMENTS

We thank Prof. K. Baldwin, T. Tang, Prof. H. Sook Sul, R. Fletcher, and Prof. Daniela Kaufer for training and advice. We thank Prof. Margolis for providing the OMP antibody. We also thank H. Dexai for assistance with tissue sectioning and P.J. Rene for help with data analysis. This work was supported by the Howard Hughes Medical Institute and the Glenn Center for Research on Aging, the American Diabetes Association Pathway to Stop Diabetes Grant 1-15-INI-12 (CER). A.D. is cofounder of Proteostasis Therapeutics, Inc., and Mitobridge, Inc., and declares no financial interest related to this work.

Received: October 7, 2016
Revised: April 9, 2017
Accepted: June 16, 2017
Published: July 5, 2017

REFERENCES

Albrecht, J., Schreder, T., Kleemann, A.M., Schöpf, V., Kopietz, R., Anzinger, A., Demmel, M., Linn, J., Kettenmann, B., and Wiesmann, M. (2009). Olfactory detection thresholds and pleasantness of a food-related and a non-food odour in hunger and satiety. Rhinology *47*, 160–165.

Bader, A., Klein, B., Breer, H., and Strotmann, J. (2012). Connectivity from OR37 expressing olfactory sensory neurons to distinct cell types in the hypothalamus. Front. Neural Circuits *6*, 84.

Balthasar, N., Coppari, R., McMinn, J., Liu, S.M., Lee, C.E., Tang, V., Kenny, C.D., McGovern, R.A., Chua, S.C., Jr., Elmquist, J.K., and Lowell, B.B. (2004). Leptin receptor signaling in POMC neurons is required for normal body weight homeostasis. Neuron *42*, 983–991.

Bartness, T.J., and Song, C.K. (2007). Thematic review series: adipocyte biology. Sympathetic and sensory innervation of white adipose tissue. J. Lipid Res. *48*, 1655–1672.

Baskin, D.G., Porte, D., Jr., Guest, K., and Dorsa, D.M. (1983). Regional concentrations of insulin in the rat brain. Endocrinology *112*, 898–903.

Belgardt, B.F., and Brüning, J.C. (2010). CNS leptin and insulin action in the control of energy homeostasis. Ann. N Y Acad. Sci. *1212*, 97–113.

Belluscio, L., Gold, G.H., Nemes, A., and Axel, R. (1998). Mice deficient in G(olf) are anosmic. Neuron *20*, 69–81.

Betley, J.N., Xu, S., Cao, Z.F.H., Gong, R., Magnus, C.J., Yu, Y., and Sternson, S.M. (2015). Neurons for hunger and thirst transmit a negative-valence teaching signal. Nature *521*, 180–185.

Bjorklund, A., Hokfelt, T., and Swanson, L.W. (1996). Integrated Systems of the CNS, Part III: Cerebellum, Basal Ganglia, Olfactory System (Elsevier).

Bonfils, P., Avan, P., Faulcon, P., and Malinvaud, D. (2005). Distorted odorant perception: analysis of a series of 56 patients with parosmia. Arch. Otolaryngol. Head Neck Surg. *131*, 107–112.

Brunet, L.J., Gold, G.H., and Ngai, J. (1996). General anosmia caused by a targeted disruption of the mouse olfactory cyclic nucleotide-gated cation channel. Neuron *17*, 681–693.

Buch, T., Heppner, F.L., Tertilt, C., Heinen, T.J.A.J., Kremer, M., Wunderlich, F.T., Jung, S., and Waisman, A. (2005). A Cre-inducible diphtheria toxin receptor mediates cell lineage ablation after toxin administration. Nat. Methods *2*, 419–426.

Buiakova, O.I., Baker, H., Scott, J.W., Farbman, A., Kream, R., Grillo, M., Franzen, L., Richman, M., Davis, L.M., Abbondanzo, S., et al. (1996). Olfactory marker protein (OMP) gene deletion causes altered physiological activity of olfactory sensory neurons. Proc. Natl. Acad. Sci. USA *93*, 9858–9863.

Cameron, J.D., Goldfield, G.S., and Doucet, É. (2012). Fasting for 24 h improves nasal chemosensory performance and food palatability in a related manner. Appetite *58*, 978–981.

Carmen, G.-Y., and Víctor, S.-M. (2006). Signalling mechanisms regulating lipolysis. Cell. Signal. *18*, 401–408.

Chaker, Z., Aïd, S., Berry, H., and Holzenberger, M. (2015). Suppression of IGF-I signals in neural stem cells enhances neurogenesis and olfactory function during aging. Aging Cell *14*, 847–856.

Chen, H., Kohno, K., and Gong, Q. (2005). Conditional ablation of mature olfactory sensory neurons mediated by diphtheria toxin receptor. J. Neurocytol. *34*, 37–47.

Chen, Y., Lin, Y.-C., Kuo, T.-W., and Knight, Z.A. (2015). Sensory detection of food rapidly modulates arcuate feeding circuits. Cell *160*, 829–841.

Clemmons, D.R. (2004). The relative roles of growth hormone and IGF-1 in controlling insulin sensitivity. J. Clin. Invest. *113*, 25–27.

Collins, S., Kuhn, C.M., Petro, A.E., Swick, A.G., Chrunyk, B.A., and Surwit, R.S. (1996). Role of leptin in fat regulation. Nature *380*, 677.

Cousin, B., Cinti, S., Morroni, M., Raimbault, S., Ricquier, D., Pénicaud, L., and Casteilla, L. (1992). Occurrence of brown adipocytes in rat white adipose tissue: molecular and morphological characterization. J. Cell Sci. *103*, 931–942.

Cowley, M.A., Smart, J.L., Rubinstein, M., Cerdán, M.G., Diano, S., Horvath, T.L., Cone, R.D., and Low, M.J. (2001). Leptin activates anorexigenic POMC neurons through a neural network in the arcuate nucleus. Nature *411*, 480–484.

Critchley, H.D., and Rolls, E.T. (1996). Hunger and satiety modify the responses of olfactory and visual neurons in the primate orbitofrontal cortex. J. Neurophysiol. *75*, 1673–1686.

Dulac, C., and Torello, A.T. (2003). Molecular detection of pheromone signals in mammals: from genes to behaviour. Nat. Rev. Neurosci. *4*, 551–562.

Elmquist, J.K., Bjørbaek, C., Ahima, R.S., Flier, J.S., and Saper, C.B. (1998). Distributions of leptin receptor mRNA isoforms in the rat brain. J. Comp. Neurol. *395*, 535–547.

Enerbäck, S., Jacobsson, A., Simpson, E.M., Guerra, C., Yamashita, H., Harper, M.E., and Kozak, L.P. (1997). Mice lacking mitochondrial uncoupling protein are cold-sensitive but not obese. Nature *387*, 90–94.

Fan, W., Boston, B.A., Kesterson, R.A., Hruby, V.J., and Cone, R.D. (1997). Role of melanocortinergic neurons in feeding and the agouti obesity syndrome. Nature *385*, 165–168.

Fernández, A.M., Kim, J.K., Yakar, S., Dupont, J., Hernandez-Sanchez, C., Castle, A.L., Filmore, J., Shulman, G.I., and Le Roith, D. (2001). Functional inactivation of the IGF-I and insulin receptors in skeletal muscle causes type 2 diabetes. Genes Dev. *15*, 1926–1934.

Ferré, P., Leturque, A., Burnol, A.F., Penicaud, L., and Girard, J. (1985). A method to quantify glucose utilization in vivo in skeletal muscle and white adipose tissue of the anaesthetized rat. Biochem. J. *228*, 103–110.

Fisher, S.J., and Kahn, C.R. (2003). Insulin signaling is required for insulin's direct and indirect action on hepatic glucose production. J. Clin. Invest. *111*, 463–468.

Fisher, F.M., Kleiner, S., Douris, N., Fox, E.C., Mepani, R.J., Verdeguer, F., Wu, J., Kharitonenkov, A., Flier, J.S., Maratos-Flier, E., and Spiegelman, B.M. (2012). FGF21 regulates PGC-1α and browning of white adipose tissues in adaptive thermogenesis. Genes Dev. *26*, 271–281.

Gascuel, J., Lemoine, A., Rigault, C., Datiche, F., Benani, A., Penicaud, L., and Lopez-Mascaraque, L. (2012). Hypothalamus-olfactory system crosstalk: orexin a immunostaining in mice. Front. Neuroanat. *6*, 44.

Getchell, T.V., Kwong, K., Saunders, C.P., Stromberg, A.J., and Getchell, M.L. (2006). Leptin regulates olfactory-mediated behavior in ob/ob mice. Physiol. Behav. *87*, 848–856.

Gogos, J.A., Osborne, J., Nemes, A., Mendelsohn, M., and Axel, R. (2000). Genetic ablation and restoration of the olfactory topographic map. Cell *103*, 609–620.

Grill, H.J., and Hayes, M.R. (2012). Hindbrain neurons as an essential hub in the neuroanatomically distributed control of energy balance. Cell Metab. *16*, 296–309.

Gropp, E., Shanabrough, M., Borok, E., Xu, A.W., Janoschek, R., Buch, T., Plum, L., Balthasar, N., Hampel, B., Waisman, A., et al. (2005). Agouti-related peptide-expressing neurons are mandatory for feeding. Nat. Neurosci. *8*, 1289–1291.

Hahn, T.M., Breininger, J.F., Baskin, D.G., and Schwartz, M.W. (1998). Coexpression of Agrp and NPY in fasting-activated hypothalamic neurons. Nat. Neurosci. *1*, 271–272.

Harrow, J., Frankish, A., Gonzalez, J.M., Tapanari, E., Diekhans, M., Kokocinski, F., Aken, B.L., Barrell, D., Zadissa, A., Searle, S., et al. (2012). GENCODE: the reference human genome annotation for The ENCODE Project. Genome Res. *22*, 1760–1774.

Haynes, W.G., Morgan, D.A., Walsh, S.A., Mark, A.L., and Sivitz, W.I. (1997). Receptor-mediated regional sympathetic nerve activation by leptin. J. Clin. Invest. *100*, 270–278.

Henkin, R.I., and Smith, F.R. (1971). Appetite and anosmia. Lancet *1*, 1352–1353.

Hill, J.M., Lesniak, M.A., Pert, C.B., and Roth, J. (1986). Autoradiographic localization of insulin receptors in rat brain: prominence in olfactory and limbic areas. Neuroscience *17*, 1127–1138.

Huszar, D., Lynch, C.A., Fairchild-Huntress, V., Dunmore, J.H., Fang, Q., Berkemeier, L.R., Gu, W., Kesterson, R.A., Boston, B.A., Cone, R.D., et al. (1997). Targeted disruption of the melanocortin-4 receptor results in obesity in mice. Cell *88*, 131–141.

Kang, N., Kim, H., Jae, Y., Lee, N., Ku, C.R., Margolis, F., Lee, E.J., Bahk, Y.Y., Kim, M.-S., and Koo, J. (2015). Olfactory marker protein expression is an indicator of olfactory receptor-associated events in non-olfactory tissues. PLoS ONE *10*, e0116097.

Kim, D., Pertea, G., Trapnell, C., Pimentel, H., Kelley, R., and Salzberg, S.L. (2013). TopHat2: accurate alignment of transcriptomes in the presence of insertions, deletions and gene fusions. Genome Biol. *14*, R36.

Könner, A.C., Janoschek, R., Plum, L., Jordan, S.D., Rother, E., Ma, X., Xu, C., Enriori, P., Hampel, B., Barsh, G.S., et al. (2007). Insulin action in AgRP-expressing neurons is required for suppression of hepatic glucose production. Cell Metab. *5*, 438–449.

Lacroix, M.-C., Badonnel, K., Meunier, N., Tan, F., Schlegel-Le Poupon, C., Durieux, D., Monnerie, R., Baly, C., Congar, P., Salesse, R., and Caillol, M. (2008). Expression of insulin system in the olfactory epithelium: first approaches to its role and regulation. J. Neuroendocrinol. *20*, 1176–1190.

Lafontan, M., and Langin, D. (2009). Lipolysis and lipid mobilization in human adipose tissue. Prog. Lipid Res. *48*, 275–297.

Li, J., Ishii, T., Feinstein, P., and Mombaerts, P. (2004). Odorant receptor gene choice is reset by nuclear transfer from mouse olfactory sensory neurons. Nature *428*, 393–399.

Li, H., Handsaker, B., Wysoker, A., Fennell, T., Ruan, J., Homer, N., Marth, G., Abecasis, G., and Durbin, R.; 1000 Genome Project Data Processing Subgroup (2009). The sequence alignment/map format and SAMtools. Bioinformatics *25*, 2078–2079.

Love, M.I., Huber, W., and Anders, S. (2014). Moderated estimation of fold change and dispersion for RNA-seq data with DESeq2. Genome Biol. *15*, 550.

Lumeng, C.N., Deyoung, S.M., Bodzin, J.L., and Saltiel, A.R. (2007). Increased inflammatory properties of adipose tissue macrophages recruited during diet-induced obesity. Diabetes *56*, 16–23.

Luquet, S., Perez, F.A., Hnasko, T.S., and Palmiter, R.D. (2005). NPY/AgRP neurons are essential for feeding in adult mice but can be ablated in neonates. Science *310*, 683–685.

Madisen, L., Zwingman, T.A., Sunkin, S.M., Oh, S.W., Zariwala, H.A., Gu, H., Ng, L.L., Palmiter, R.D., Hawrylycz, M.J., Jones, A.R., et al. (2010). A robust and high-throughput Cre reporting and characterization system for the whole mouse brain. Nat. Neurosci. *13*, 133–140.

Margolis, F.L., Verhaagen, J., Biffo, S., Huang, F.L., and Grillo, M. (1991). Regulation of gene expression in the olfactory neuroepithelium: a neurogenetic matrix. Prog. Brain Res. *89*, 97–122.

Marino, J.S., Xu, Y., and Hill, J.W. (2011). Central insulin and leptin-mediated autonomic control of glucose homeostasis. Trends Endocrinol. Metab. *22*, 275–285.

McIntyre, J.C., Titlow, W.B., and McClintock, T.S. (2010). Axon growth and guidance genes identify nascent, immature, and mature olfactory sensory neurons. J. Neurosci. Res. *88*, 3243–3256.

McIntyre, J.C., Davis, E.E., Joiner, A., Williams, C.L., Tsai, I.-C., Jenkins, P.M., McEwen, D.P., Zhang, L., Escobado, J., Thomas, S., et al.; NISC Comparative Sequencing Program (2012). Gene therapy rescues cilia defects and restores olfactory function in a mammalian ciliopathy model. Nat. Med. *18*, 1423–1428.

Nickell, M.D., Breheny, P., Stromberg, A.J., and McClintock, T.S. (2012). Genomics of mature and immature olfactory sensory neurons. J. Comp. Neurol. *520*, 2608–2629.

Obici, S., Zhang, B.B., Karkanias, G., and Rossetti, L. (2002). Hypothalamic insulin signaling is required for inhibition of glucose production. Nat. Med. *8*, 1376–1382.

Palouzier-Paulignan, B., Lacroix, M.-C., Aimé, P., Baly, C., Caillol, M., Congar, P., Julliard, A.K., Tucker, K., and Fadool, D.A. (2012). Olfaction under metabolic influences. Chem. Senses *37*, 769–797.

Petrovic, N., Walden, T.B., Shabalina, I.G., Timmons, J.A., Cannon, B., and Nedergaard, J. (2010). Chronic peroxisome proliferator-activated receptor gamma (PPARgamma) activation of epididymally derived white adipocyte cultures reveals a population of thermogenically competent, UCP1-containing adipocytes molecularly distinct from classic brown adipocytes. J. Biol. Chem. *285*, 7153–7164.

Pixley, S.K., Dangoria, N.S., Odoms, K.K., and Hastings, L. (1998). Effects of insulin-like growth factor 1 on olfactory neurogenesis in vivo and in vitro. Ann. N Y Acad. Sci. *855*, 244–247.

Pocai, A., Obici, S., Schwartz, G.J., and Rossetti, L. (2005). A brain-liver circuit regulates glucose homeostasis. Cell Metab. *1*, 53–61.

Purves, D., Augustine, G.J., Fitzpatrick, D., Katz, L.C., LaMantia, A.-S., McNamara, J.O., and Williams, S.M. (2001). The Organization of the Olfactory System (Sinauer Associates).

Rahmouni, K., and Morgan, D.A. (2007). Hypothalamic arcuate nucleus mediates the sympathetic and arterial pressure responses to leptin. Hypertension *49*, 647–652.

Savigner, A., Duchamp-Viret, P., Grosmaitre, X., Chaput, M., Garcia, S., Ma, M., and Palouzier-Paulignan, B. (2009). Modulation of spontaneous and odorant-evoked activity of rat olfactory sensory neurons by two anorectic peptides, insulin and leptin. J. Neurophysiol. *101*, 2898–2906.

Seale, P., Conroe, H.M., Estall, J., Kajimura, S., Frontini, A., Ishibashi, J., Cohen, P., Cinti, S., and Spiegelman, B.M. (2011). Prdm16 determines the thermogenic program of subcutaneous white adipose tissue in mice. J. Clin. Invest. *121*, 96–105.

Shioda, S., Funahashi, H., Nakajo, S., Yada, T., Maruta, O., and Nakai, Y. (1998). Immunohistochemical localization of leptin receptor in the rat brain. Neurosci. Lett. *243*, 41–44.

Skibicka, K.P., and Grill, H.J. (2009). Hypothalamic and hindbrain melanocortin receptors contribute to the feeding, thermogenic, and cardiovascular action of melanocortins. Endocrinology *150*, 5351–5361.

Soria-Gómez, E., Bellocchio, L., Reguero, L., Lepousez, G., Martin, C., Bendahmane, M., Ruehle, S., Remmers, F., Desprez, T., Matias, I., et al. (2014). The endocannabinoid system controls food intake via olfactory processes. Nat. Neurosci. *17*, 407–415.

Spencer, S.E., Sawyer, W.B., Wada, H., Platt, K.B., and Loewy, A.D. (1990). CNS projections to the pterygopalatine parasympathetic preganglionic

neurons in the rat: a retrograde transneuronal viral cell body labeling study. Brain Res. *534*, 149–169.

Stachelscheid, H., Ibrahim, H., Koch, L., Schmitz, A., Tscharntke, M., Wunderlich, F.T., Scott, J., Michels, C., Wickenhauser, C., Haase, I., et al. (2008). Epidermal insulin/IGF-1 signalling control interfollicular morphogenesis and proliferative potential through Rac activation. EMBO J. *27*, 2091–2101.

Stephan, A.B., Tobochnik, S., Dibattista, M., Wall, C.M., Reisert, J., and Zhao, H. (2011). The Na(+)/Ca(2+) exchanger NCKX4 governs termination and adaptation of the mammalian olfactory response. Nat. Neurosci. *15*, 131–137.

Su, C.-Y., Menuz, K., and Carlson, J.R. (2009). Olfactory perception: receptors, cells, and circuits. Cell *139*, 45–59.

Sultan, M., Dökel, S., Amstislavskiy, V., Wuttig, D., Sültmann, H., Lehrach, H., and Yaspo, M.-L. (2012). A simple strand-specific RNA-Seq library preparation protocol combining the Illumina TruSeq RNA and the dUTP methods. Biochem. Biophys. Res. Commun. *422*, 643–646.

Tsukiyama-Kohara, K., Poulin, F., Kohara, M., DeMaria, C.T., Cheng, A., Wu, Z., Gingras, A.C., Katsume, A., Elchebly, M., Spiegelman, B.M., et al. (2001). Adipose tissue reduction in mice lacking the translational inhibitor 4E-BP1. Nat. Med. *7*, 1128–1132.

Tucker, K., Overton, J.M., and Fadool, D.A. (2012). Diet-induced obesity resistance of Kv1.3$^{-/-}$ mice is olfactory bulb dependent. J. Neuroendocrinol. *24*, 1087–1095.

Vogt, M.C., and Brüning, J.C. (2013). CNS insulin signaling in the control of energy homeostasis and glucose metabolism - from embryo to old age. Trends Endocrinol. Metab. *24*, 76–84.

Wardlaw, S.L. (2011). Hypothalamic proopiomelanocortin processing and the regulation of energy balance. Eur. J. Pharmacol. *660*, 213–219.

Williams, K.W., and Elmquist, J.K. (2012). From neuroanatomy to behavior: central integration of peripheral signals regulating feeding behavior. Nat. Neurosci. *15*, 1350–1355.

Wu, J., Boström, P., Sparks, L.M., Ye, L., Choi, J.H., Giang, A.-H., Khandekar, M., Virtanen, K.A., Nuutila, P., Schaart, G., et al. (2012). Beige adipocytes are a distinct type of thermogenic fat cell in mouse and human. Cell *150*, 366–376.

Wu, Z., Autry, A.E., Bergan, J.F., Watabe-Uchida, M., and Dulac, C.G. (2014). Galanin neurons in the medial preoptic area govern parental behaviour. Nature *509*, 325–330.

Xu, H., Barnes, G.T., Yang, Q., Tan, G., Yang, D., Chou, C.J., Sole, J., Nichols, A., Ross, J.S., Tartaglia, L.A., and Chen, H. (2003a). Chronic inflammation in fat plays a crucial role in the development of obesity-related insulin resistance. J. Clin. Invest. *112*, 1821–1830.

Xu, J., Koni, P.A., Wang, P., Li, G., Kaczmarek, L., Wu, Y., Li, Y., Flavell, R.A., and Desir, G.V. (2003b). The voltage-gated potassium channel Kv1.3 regulates energy homeostasis and body weight. Hum. Mol. Genet. *12*, 551–559.

Yakar, S., Liu, J.-L., Fernandez, A.M., Wu, Y., Schally, A.V., Frystyk, J., Chernausek, S.D., Mejia, W., and Le Roith, D. (2001). Liver-specific igf-1 gene deletion leads to muscle insulin insensitivity. Diabetes *50*, 1110–1118.

Yang, C.F., Chiang, M.C., Gray, D.C., Prabhakaran, M., Alvarado, M., Juntti, S.A., Unger, E.K., Wells, J.A., and Shah, N.M. (2013). Sexually dimorphic neurons in the ventromedial hypothalamus govern mating in both sexes and aggression in males. Cell *153*, 896–909.

Yoon, H., Enquist, L.W., and Dulac, C. (2005). Olfactory inputs to hypothalamic neurons controlling reproduction and fertility. Cell *123*, 669–682.

Young, P., Arch, J.R., and Ashwell, M. (1984). Brown adipose tissue in the parametrial fat pad of the mouse. FEBS Lett. *167*, 10–14.

STAR★METHODS

KEY RESOURCES TABLE

REAGENT or RESOURCE	SOURCE	IDENTIFIER
Antibodies		
anti-GAP43	Cell Signaling	sc-17790
anti-Gα olf	Santa Cruz Biotechnology	sc-383
anti-GFP	Thermo Fisher	A-6455
anti-HSL	Cell Signaling	#18381
anti-iba1	Wako	#019-19741
anti-Kcnq2	Cell Signaling	sc-7793
anti-mCherry	Thermo Fisher	PA5-34974
anti-OMP	Wako	
anti-p-HSL Ser 660	Cell Signaling	#4126
anti-tubulin	Cell Signaling	#2144
Bacterial and Virus Strains		
pAAV-flex-taCasp3-TEVp	Nirao Shah & Jim Wells	Addgene plasmid # 45580
AdGFP	Jeremy McIntyre (Univ of Florida) McIntyre et al., 2012	N/A
Chemicals, Peptides, and Recombinant Proteins		
2-deoxy-D-[1-14C] glucose (2DG)	Amersham	CAS: #154-17-6
BSA	Sigma	A8806
Complete protease inhibitor tablet	Roche	11697498001
D-[3-3H] glucose	Amersham Biosciences	CAS: #2535-38-8
Humulin	Eli Lilly	
IGF1R transcript	ACD; Advanced Cell Diagnostics Inc., Hayward, CA	target region: 1231-1554, Acc. No. NM_010513.2
Insulin	Roche	#11376497001
Insulin	Novo Nordisk	
Isoproterenol	Sigma-Aldrich	CAS: #51-30-9
OCT	Tissue-Tek	VWR CAT #25608-930
PhosSTOP	Roche	4906845001
VECTOR Hematoxylin QS	Vector laboratories, Burlingame, CA	#H-3404
Critical Commercial Assays		
UltraSensitive Insulin ELISA kit	Crystal Chem	#90080
Free Glycerol Determination kit	Sigma-Aldrich	FG0100-1KT
Quantikine ELISA kit	R&D systems	
Noradrenaline sensitive ELISA kit	Eagle Biosciences	SKU: NOU39-K01
Virapur Adenovirus mini purification Virakit	Virapur, San Diego, CA	
Experimental Models: Organisms/Strains		
Mouse: OMP Cre, B6;129P2-Omptm4(cre) Mom/MomJ	https://www.jax.org/strain/006668	Stock Nr: 006668
Mouse: iDTR	Buch et al., 2005	N/A
Mouse: IGF1Rfl/fl, Igf1r^{tm2Arge}	https://www.jax.org/strain/012251	012251
Mouse: TdTomato, B6;129S6-Gt(ROSA) 26Sor$^{tm9(CAG-tdTomato)Hze}$/J	Madisen et al., 2010	N/A
Oligonucleotides		
See Table S1		

(*Continued on next page*)

Continued

REAGENT or RESOURCE	SOURCE	IDENTIFIER
Software and Algorithms		
Deseq2	Love et al., 2014	https://bioconductor.org/packages/release/bioc/html/DESeq2.html
GENCODE		https://www.gencodegenes.org
GraphPad Prism 5		https://www.graphpad.com/scientific-software/prism/
org.Mm.eg.db	Bioconductor	http://bioconductor.org/packages/release/data/annotation/html/org.Mm.eg.db.html
RStudio	RStudio	https://www.rstudio.com
samtools	Li et al., 2009	http://samtools.sourceforge.net
SeqMonk	Babraham Bioinformatics	https://www.bioinformatics.babraham.ac.uk/projects/seqmonk/
topGO	Bioconductor	https://bioconductor.org/packages/release/bioc/html/topGO.html
Tophat2		https://ccb.jhu.edu/software/tophat/index.shtml
Trim Galore!	Babraham Bioinformatics	https://www.bioinformatics.babraham.ac.uk/projects/trim_galore/

CONTACT FOR REAGENT AND RESOURCE SHARING

As Lead Contact, Andrew Dillin is responsible for all reagent and resource requests. Please contact Andrew Dillin at dillin@berkeley.edu with requests and inquiries.

METHOD DETAILS

Animal Care

All procedures were approved by the Animal Care and Use Committee of UC Berkeley and MPI Cologne. Mice were housed at 22°C–24°C using a 12 hr light/12 hr dark cycle. Animals had ad libitum access to water at all times, and food was only withdrawn if required for an experiment. All experiments have been performed in adult mice.

Genetic mouse models

All animals described in this study have been generated elsewhere and described in the key resource table. Ablation of mature olfactory neurons in adult mice was achieved by expressing the inducible diphteria toxin receptor (DTR) specifically in OSNs and conditional ablation by diphtheria toxin (DT) administration as previously described (Chen et al., 2005). Heterozygous mice expressing the Cre recombinase under the olfactory marker protein (OMP) promoter were crossed to homozygous mice expressing DTR under a ubiquitously active promoter blocked by loxP-stop flanking cassette (Buch et al., 2005; Gropp et al., 2005) to generate OMP-DTR$^{+/-}$ (OMP^{DTR}) and DTR$^{+/-}$ (control) animals (Figure 1a). OMP-DTR$^{+/-}$ and DTR$^{+/-}$ littermates were generated from 5 breeders pairs of homozygous DTR$^{-/-}$ mutant mice crossed to OMP-Cre mice in the C57BL/6J background obtained from the Jackson laboratory (Bar Harbor, ME). DT (40ng/g) was administered intraperitoneally every 3 weeks to maintain olfactory ablation. For DIO, all male mice were fed a normal chow (PicoLab Rodent 20 5053*, LabDiet) until 6 weeks of age. Subsequently, mice were assigned randomly to either HFD chow (BioServ, 60% fat calories) or control chow (BioServ, 7% fat calories). IGF1R$^{flox/flox}$ mice (Stachelscheid et al., 2008) were crossed to OMP-Cre mice in order to obtain control (IGF1Rfl/fl) and IGF1RΔOMP (IGF1Rfl/flOMPCre+/−) mice. For immunohistochemistry mice were crossed to tdTomato reporter (B6;129S6-Gt(ROSA)26Sor$^{tm9(CAG-tdTomato)Hze}$/J (Madisen et al., 2010) to obtain tdTomato;ΔOMP (tdTomato$^{+/-}$;ΔOMP$^{+/-}$) and IGF1R;tdTomatoΔOMP (IGF1Rfl/fl;tdTomato$^{+/-}$;OMP$^{+/-}$) mice.

Indirect Calorimetry, Physical Activity, and Food Intake

Indirect calorimetric studies were conducted in a Comprehensive Lab Animal Monitoring System in an eight-chamber system (CLAMS, Columbus Instruments) at UC Berkeley and PhenoMaster System (TSE systems) at MPI. Body composition was assessed by EchoMRI and NMR Analyzer minispeq mq7.5 (Bruker Optik). Mice were allowed to acclimatize in the chambers for at least 24 hr. Food and water were provided ad libitum in the appropriate devices and measured by the built-in automated instruments. Locomotor activity and parameters of indirect calorimetry were measured for at least the following 48 hr. Presented data are average values obtained in these recordings.

Food finding test

The mice were single caged a week before the experiment started. They were habituated to the small food pellets, the perforated eppendorf tube and the round buckets that were used during the experiment. The experiment took place in three consecutive days with two trials per day. The mice were given up to 15 min to find the hidden under 4cm of bedding perforated eppendorf tube containing the food pellets.

Social odor finding test

Urine was collected from ten female mice. A q-tip was dipped in the urine and placed in a perforated Eppendorf tube which was hidden under 4cm of bedding in a round bucket. The mice were given up to 15 min to find the hidden perforated Eppendorf tube containing the food pellets hidden under 4 cm of bedding.

Habituation-dishabituation test

The mice were exposed to five smells in three consecutive 2min trials per smell. The time that the mouse spent with its nose 2cm or closer to the odor source was measured using an automated camera system.

Metabolic studies

To perform the GTT, mice were fasted for 6h and tails were bled for the initial blood glucose concentration measured using a One Touch Ultra glucometer (LifeScan) or Bayer Contour glucometer (Bayer). Glucose (2g/kg weight) was intraperitoneally administered and blood glucose was measured at indicated times after injection. For the ITT, 5 hr fasted mice were injected with 0.75-1u/kg of human insulin (Humulin; Eli Lily, Roche or Novo Nordisk) and glucose was measured as in the GTT. Serum insulin was measured using an UltraSensitive Insulin ELISA kit (Crystal Chem). Serum levels of fasted leptin were measured using a Quantikine ELISA Kits (R&D systems). Noradrenaline were measured using a sensitive ELISA Kits (Eagle Biosciences), and fasted levels of free fatty acids were measured using a Free Fatty Acid Quantitation Kit (Sigma Aldrich). To measure Phospho (Ser 660) HSL levels in WAT, Isoproterenol (10mg/kg) or saline was injected intraperitoneally 15 min prior to animal's euthanasia.

Ex vivo lipolysis

Gonadal fat pads were isolated from mice and weighed. Each pad was cut into 3 equal pieces and incubated in Krebs-Ringer Bicarbonate Buffer containing 1% fatty acid–free BSA (Sigma-Aldrich). The samples were treated with either PBS or isoproterenol (25 μM, Sigma-Aldrich) at 37°C with mild shaking at 300 rpm. After 120 min, glycerol release was measured using the Free Glycerol Determination Kit (Sigma-Aldrich).

Protein analysis

Adipose tissue was homogenized in TNET buffer (50mM Tris-HCl, 5mM EDTA, 150mM NaCl), supplemented with Complete protease inhibitor tablet (Roche), PhosSTOP (Roche). Protein concentrations were determined using Bradford. 20-50μg of samples were loaded on SDS/Page gels (Invitrogen) then transferred to nitrocellulose membranes. Ponceau S staining was used to confirm equal loading. Immunoblotting was done in 3% BSA containing TBS-T with antibodies against Phospho HSL (Ser 660), HSL, α-tubulin.

Leptin sensitivity

Recombinant mouse leptin (R&D systems) was injected intraperitoneally 90 min before the onset of the dark cycle for 3 consecutive days (3 mg/kg) in an independent cohort of obese OMP^{DTR} and control animals, before and 2 weeks post DT delivery. Food intake and body weights were recorded daily.

Quantitative PCR analysis

RNA was isolated using trizol/chloroform extraction and RNEasy QIAGEN columns. RNA was converted into cDNA using quantitect reverse-transcription kit. Gene expression was assessed by qPCR using SYBR green.

Adenovirus propagation and titration

All adenoviruses used in this study are replication-deficient (E1 deleted), serotype 5 adenovirus, and were produced following the ViraPower protocol (Invitrogen). The amplified virus was purified with the Virapur Adenovirus mini purification Virakit (Virapur, San Diego, CA), which was followed by dialyzation into a solution of 2.5% glycerol, 25 mM NaCl and 20 mM Tris-HCl, pH 8.0, at 4°C overnight before storing it at −80°C. AdGFP was a gift from Jeremy McIntyre (Univ of Florida)(McIntyre et al., 2012), and Ad-taCasp3-TEVp under the EF-1a promoter was subcloned from AAV-flex-taCasp3-TEVp (Yang et al., 2013) and inserted into the adenoviral vector pAD/PL-DEST (Invitrogen). pAAV-flex-taCasp3-TEVp was a gift from Nirao Shah & Jim Wells (Addgene plasmid # 45580). Stock titrations were: Ad-GFP, 1.11×10^{12} particles per mL; Ad-taCasp3, 1.10×10^{12} particles per mL.

Immunofluorescence and histological studies

Whole mouse heads were fixed in 4% paraformaldehyde, then decalcified in 10% ethylenediaminetetraacetic acid dissolved in PBS at pH 7.6 for 2-3 weeks to perform olfactory epithelium staining. Tissues were cryoprotected in 30% sucrose in PBS overnight, then frozen in OCT (Tissue-Tek) and sectioned on a cryostat. 12-20 μm thick sections were immunoblotted with primary antibodies in PBS

containing 2% Donkey serum and 0.4% Triton x100. Antibodies used were diluted at 1:100 or 1:200 and secondary antibodies (Alexxa) were diluted at 1:600. Sections were imaged using a LSM 710 confocal microscope and a Keyence microscope BZ-X700. For quantification of OMP+ cells, coronal sections of MOE lining the septum were chosen. Semi-quantification for OMP+ cells were measured by point-counting morphometry using the VS-ASW software. For histological analysis, tissues were immersed in formalin overnight, dried in 70% Ethanol and embedded in paraffin. 8μm thick sections were stained with hematoxylin and eosin and finally imaged with a VS120 slide scanner (Olympus).

Hyperinsulinemic-euglycemic CLAMPS

Catheter implantation in the jugular vein was performed as previously described (Fisher and Kahn, 2003). Only mice that had regained at least 90% of their preoperative body weight after 6 days of recovery were included in the experimental groups. After starvation for 4 hr the clamp was performed in awake animals. After a bolus infusion (5 μCi) of D-[3-3H] glucose (Amersham Biosciences) tracer solution, the tracer was infused continuously (0.05 μCi/min) for the duration of the experiment. At the end of the 50 min basal period, a blood sample (50 μl) was collected for determination of basal parameters. Insulin (human regular insulin; Novo Nordisk) solution containing 0.1% BSA (Sigma) was infused at a fixed rate (4 μU/g/min) following a bolus infusion (20 μU/g). Blood glucose levels were determined every 10 min (B-Glucose Analyzer, HemoCue), and physiological blood glucose levels (between 120 and 145 mg/dl) were maintained by adjusting a 20% glucose infusion (DeltaSelect). 60 min after the insulin bolus infusion, which coincides approximately to 60 min before steady state was achieved, a bolus of 2-deoxy-D-[1-14C] glucose (2DG) (10 μCi, Amersham) was infused. Steady state was ascertained when glucose measurements were constant for at least 30 min at a fixed glucose infusion rate and was achieved within 100 to 130 min. During the clamp experiment, blood samples (15 μl) were collected after infusion of the 2DG at time points 0, 5, 15, 25, 35 min, etc. until reaching the steady state. During the steady state, blood samples (50 μl) were collected for the measurement of steady-state parameters. All blood samples were kept at room temperature until centrifugation; serum samples were stored at −20°C. At the end of the experiment, mice were euthanized by cervical dislocation, and brain, liver, white adipose tissue (WAT), and skeletal muscle were dissected and stored at −80°C.

Plasma [3-3H] glucose radioactivity at basal and steady state was measured as previously described (Fisher and Kahn, 2003). Plasma deoxy-[1-14C] glucose radioactivity was directly measured in a liquid scintillation counter. WAT and skeletal muscle lysates were processed through ion-exchange chromatography columns (Poly-Prep Prefilled Chromatography Columns, AG1-X8 formate resin, 200–400 mesh dry; Bio-Rad) to separate 2DG from 2DG-6-phosphate (2DG6P).

Glucose turnover rate (mg/kg/min) was calculated as previously described (Fisher and Kahn, 2003). In vivo glucose uptake for brain, WAT, and skeletal muscle (nmol/g/min) based on the accumulation of 2DG6P in the respective tissue and the disappearance rate of 2DG from plasma was calculated as described previously (Ferré et al., 1985).

Adipose tissue oxygen consumption

Adipose tissue was minced into small pieces and rinsed two times with PBS through a 100 μm strainer. 10 mg of tissue was placed into each well of an XF24-well Islet Flux plate (Seahorse Bioscience). Tissue chunks were washed with 1 mL of assay media (1x KHB, 2.5mM glucose, 0.5mM carnitine, 0.5mM HEPES, 0.24mM $MgCl_2$; pH to 7.4 at 37°C), then 450 μL of fresh assay media was added to every well and plate was run in Seahorse XF-24 (mix 3 min, wait 2 min, measure 3min). Results of OCR and ECAR were normalized to protein concentration.

Bomb fecal calorimetry

Freeze-dried feces was pooled and pulverized with a ceramic mortar and pestle. Caloric content of feces was measured with an 1108 Oxygen Combustion Bomb calorimeter and normalized to replicate benzoic acid standards. n = replicate explosion of pooled feces.

RNA sequencing

RNA-seq library preparation and measurement was performed by the Cologne Center for Genomics, Cologne, Germany. Stranded TruSeq RNA-seq library preparation was principally conducted as previously described (Sultan et al., 2012) with 2 μg of extracted RNA and poly-A enrichment. Barcoded libraries were sequenced with 100 bp paired-end reads on an Illumina HiSeq2500. Raw sequence reads were trimmed to remove adaptor contamination and poor-quality reads using Trim Galore! (v0.3.7, parameters:–paired–length 25). Trimmed sequences were aligned using Tophat2 (Kim et al., 2013) (v2.0.14, parameters:–no-mixed–library-type = fr-firststrand -g 2 -r 500–mate-std-dev 525) against the mouse reference genome (build GRCm38), supplying GENCODE annotation (Harrow et al., 2012) (release M2, main annotation) for improved mapping. Multi-mapped reads were filtered using samtools (Li et al., 2009) (v1.2, parameters: view -F 0x100 -b –h). Data visualization and analysis was performed using SeqMonk, custom RStudio and the following Bioconductor packages: Deseq2 (Love et al., 2014), topGO and org.Mm.eg.db. To account for tissue specific expression, we defined all genes with an FPKM of > 2 in at least half of all samples as 'expressed'. Unless stated otherwise, the set of expressed genes was used as background for all conducted functional enrichment analyses with topGO. For determining the maturity state of olfactory neurons, a previously published study (Nickell et al., 2012) was used as reference. Mature and immature marker genes lists were used to calculate the enrichment among the entire set of significant differentially expressed genes (p-val < 0.05 after running Deseq2) as well as enrichments among the respective sub-populations of up- and downregulated genes, using one-sided Fisher's exact test. Additionally, random subsets of the same size as the immature/mature

marker sets were drawn out of all significant differentially expressed genes and their respective log2foldchange distributions were compared to the two distributions of the immature/mature marker set.

RNAscope analysis

Chromogenic in situ hybridization for the detection of IGF1R was performed using RNAscope (ACD; Advanced Cell Diagnostics Inc., Hayward, CA). A custom designed probe targeting the floxed region (exon 3) of the IGF1R transcript (target region: 1231-1554, Acc. No. NM_010513.2). Negative and positive control probes recognizing dihydrodipicolinate reductase, DapB (a bacterial transcript) and cyclophilin (PPIB), respectively, were processed in parallel with the target probe to ensure tissue RNA integrity and optimal assay performance. All pretreatment reagents, detection kit and wash buffer were purchased from ACD. All incubation steps at 40°C were performed using a humidified chamber and a HybEz oven (ACD).

The day before the assay, slides were removed from the −80 freezer, allowed to thaw and were then washed for 5 min in 0.1 M phosphate buffered saline (PBS, pH 7.4) in order to remove tissue embedding medium. Slides were then briefly dipped in diethylpyrocarbonate (DEPC) treated Millipore water and allowed to dry at room temperature, before being incubated at 60°C overnight.

On the day of the assay, the tissue underwent a pretreatment procedure to allow for optimal probe penetration and assay performance. First, sections were incubated with RNAscope Hydrogen Peroxide (ACD) for 20 min at room temperature. Slides were then submerged in Target Retrieval (ACD) for 8 min, heated to 98.5-99.5°C, followed by two brief rinses in DEPC water. The slides were quickly dehydrated in 100% ethanol and allowed to air dry for 5 min. A hydrophobic barrier was drawn around each section with an Immedge barrier pen. Each section was then incubated with Protease Plus (ACD) for 20 min at 40°C, followed by 10 min at room temperature. The subsequent steps, i.e., hybridization of the probe, the amplification steps and detection of the probe, were performed according to the online protocol for RNAscope 2.5 High Definition (HD) BROWN Assay.

In brief, the procedure included the following steps; hybridization of the IGF1R probe at 40°C for 2 hr, 2x2 min washes in Wash buffer (ACD), incubation with Amp1 at 40°C for 30 min, 2x2 min washes, Amp2 at 40°C for 15 min, 2x2 min washes, Amp3 at 40°C for 30 min, 2x2 min washes, Amp4 at 40°C for 15 min, 2x2 min washes, Amp5 at room temperature for 30 min, 2x2 min washes, Amp6 at room temperature for 15 min, 2x2 min washes, incubation in DAB substrate for 10 min at room temperature. After this step, sections were briefly washed in tap water two times, counterstained with VECTOR Hematoxylin QS (40 s; Vector laboratories, Burlingame, CA), dehydrated for 2 min each in 70%, 95% and 95% ethanol. Finally, slides were defatted in xylene for 5 min before being coverslipped with Cytoseal mounting medium.

Data and Software Availability

Transcriptome profiles of olfactory sensory neurons derived from IGF1R$^{\Delta OMP}$ mice have been deposited in the NCBI's Gene Expression Omnibus repository under ID code GSE85329: https://www.ncbi.nlm.nih.gov/geo/query/acc.cgi?acc=GSE85329.

Statistical methods

GraphPad Prism 5 was used for statistical analysis. Data are expressed as mean ± SEM p Values were calculated using unpaired two-tailed unequal variance Student's t test unless or two-way ANOVA with post hoc Bonferroni tests (when specified). P values less than 0.05 were considered significant.

Cell Metabolism, Volume *26*

Supplemental Information

The Sense of Smell Impacts Metabolic Health and Obesity

Celine E. Riera, Eva Tsaousidou, Jonathan Halloran, Patricia Follett, Oliver Hahn, Mafalda M.A. Pereira, Linda Engström Ruud, Jens Alber, Kevin Tharp, Courtney M. Anderson, Hella Brönneke, Brigitte Hampel, Carlos Daniel de Magalhaes Filho, Andreas Stahl, Jens C. Brüning, and Andrew Dillin

Supplementary figures

Figure S1. Related to Figure 1. Representative images of OMP-Cre-negative and positive Rosa26-StopFlox-CAG-tdTomato mice.

A- Native RFP fluorescence was analyzed in MOE, thyroid and thymus stained with Dapi.

B,C,D- Native RFP fluorescence was detected in olfactory bulb (B, sagittal section), hypothalamus and optic chiasm (C, coronal section), and cerebellum (D, coronal section) at 2X and 20X. Arrows indicate regions expressing RFP.

E- Immunofluorescence images of a representative coronal MOE section comparing native RFP fluorescence colocalization with an antibody raised against OMP protein. dsRed Green, OMP red, dapi blue.

Figure S2. Related to Figure 1. Efficacy of OSN ablation in OMP^{DTR} mice.

A - Immunofluorescence images of coronal MOE and VNO sections from OMP^{DTR} and control littermates following 3 DT injections. Gα olf Green, OMP red, dapi blue.

B - Average time needed to find a perforated eppendorf tube, hidden under the bedding, containing a q-tip immersed in urine of 10 female mice for random fed OMP^{DTR} and control littermates (n=5 vs 5). One trial.

C - Habituation-dishabituation test with five different odors. Average time (in sec) spent with the nose of the mouse being 2cm or closer to the odor source, each trial lasted for 2min for random fed OMP^{DTR} and control littermates (n=5 vs 5) and 3 sequential trials per odor were conducted. ***p<0.001, **p<0.001, *p<0.05, two-tailed unequal variance Student's *t* test unless specified. All values denote means ± SEM.

Figure S3. Related to Figure 3. Metabolic parameters of OMP^{DTR} mice.

A - Weight gain of DT-injected OMP^{DTR} and controls when maintained on chow diet for 8 weeks then placed on HFD (n=10vs10, ***p<0.0001, two-way ANOVA).

B- Fat mass and lean mass of OMP^{DTR} and control littermates (n=10 vs 10).

C- Cumulative food intake from a 12h fast-refeeding test in HFD-fed OMP^{DTR} and control littermates (n=6 vs 6).

D - Fecal calory content in HFD (n=10 vs 10) and normal chow (n=6 vs 5) fed OMP^{DTR} and control littermates.

E- Phospho (Ser 660) HSL, HSL, α-tubulin levels in WAT from HFD-fed OMP^{DTR} and control littermates after isoproterenol or saline injection after 14 weeks of DIO (n=3 vs 3).

F - Lipolysis rates in adipocytes exposed to Vehicle from gonadal WAT isolated from HFD-fed OMP^{DTR} and control littermates (n=3 vs 3).

G- Respiratory quotient of HFD-fed OMP^{DTR} and control littermates (n=4 vs 4)

***p<0.001, **p<0.001, *p<0.05, two-tailed unequal variance Student's *t* test unless specified. All values denote means ± SEM.

Figure S4. Related to Figure 4. Exploration of brain specific ablation in obese olfactory deficient models.

A,B - Immunofluorescence images of coronal hypothalamic sections from OMP^{DTR} and control littermates following 3 DT injections. A (dsRed red, dapi blue), B (iba-1 red, dapi blue).

C- RTqPCR against GFAP in whole CNS and hypothalami of HFD-fed OMP^{DTR} and control mice after 14 weeks of DIO (n=6 vs 5).

D- Average time needed to find a perforated eppendorf tube, hidden under the bedding, containing a q-tip immersed in urine of 10 female mice for random fed OMP-Cre+ and control OMP-Cre- littermates injected with intranasal Ad-GFP and Ad-flex-ta-Casp3-TEVp (n=5 vs 5). One trial.

E Immunofluorescence images of coronal MOB and MOE section from OMP-Cre+ receiving Ad-GFP, α- OMP (red), α- GFP (green), dapi (blue). Arrows show the limited penetrance of Ad-GFP by intranasal delivery into caudal MOE and absence in the MOB.

F- Habituation-dishabituation test with five different odors. Average time (in sec) spent with the nose of the mouse being 2cm or closer to the odor source, each trial lasted for 2min for random fed OMP^{DTR} and control littermates (n=5 vs 5) and 3 sequential trials per odor were conducted.

***p<0.001, **p<0.001, *p<0.05, two-tailed unequal variance Student's *t* test unless specified. All values denote means ± SEM.

Figure S5. Related to Figure 5. Effect of OSN ablation on metabolism in obese mice subjected to DIO.

A - Representative picture of DT-injected OMP^{DTR} and control littermates fed a HFD prior to DT administration.

B - Insulin tolerance of HFD-fed mice (n=12 vs 10) (***p<0.0001, one-way ANOVA).

C - Oxygen consumption in HFD-fed DT-injected OMP^{DTR} and control littermates (n=4 vs 4), (***p<0.0001, one-way ANOVA).

D - Fasting serum insulin levels (n=8 vs 13).

***p<0.001, **p<0.001, *p<0.05, two-tailed unequal variance Student's *t* test unless specified. All values denote means ± SEM.

Figure S6. Related to Figure 6. IGF1R is efficiently ablated in the olfactory epithelium of $IGF1R^{\Delta OMP}$ mice and results in differential mature and immature olfactory marker expression.

A - IGF1R mRNA quantification in the olfactory epithelium of control and IGF1R $^{\Delta OMP}$ mice by utilization of RNAscope. Scale bar 10μm.

B - Relative IGF1R mRNA expression by real-time PCR analysis and RNAsequencing in control and $IGF1R^{\Delta OMP}$ mice, respectively (n=4 vs 4 and 6 vs 4).

C - Relative IR mRNA expression by real-time PCR analysis and RNAsequencing in control and $IGF1R^{\Delta OMP}$ mice, respectively (n=4 vs 4 and 6 vs 4).

D - Log2 fold change of differentially expressed mature and immature olfactory markers in the olfactory epithelium of control and IGF1R $^{\Delta OMP}$ mice (n=4 vs 4).

E- Relative mRNA expression of immature, mature olfactory markers and markers of proliferation (Mki67) and apoptosis (Caspase 3, Caspase 4) in control (n=6) and $IGF1R^{\Delta OMP}$ (n=4) mice.

F- Habituation-dishabituation test with five different odors. Average time (in sec) spent with the nose of the mouse being 2cm or closer to the odor source, each trial lasted for 2min for random fed control and IGF1R $^{\Delta OMP}$ mice (n=10 vs 10) and 3 sequential trials per odor were conducted. ***p<0.001, **p<0.001, *p<0.05, two-tailed unequal variance Student's *t* test unless specified. All values denote means ± SEM.

Figure S7. Related to Figure 7. Increased immature and decreased mature olfactory marker expression in olfactory

A- Representative GAP43, an immature olfactory marker, immunostaining in olfactory epithelia of tdTomato$^{\Delta OMP}$ and IGF1R;tdTomato$^{\Delta OMP}$ mice. Scale bar 10μm.

B- Quantification of GAP43 immunostaining intensity in olfactory epithelia of tdTomato$^{\Delta OMP}$ and IGF1R;tdTomato$^{\Delta OMP}$ mice (n=3 vs 3).

C- Representative Kcnq2, a mature olfactory marker, immunostaining in olfactory epithelia of tdTomato$^{\Delta OMP}$ and IGF1R;tdTomato$^{\Delta OMP}$ mice. Scale bar 10μm.

D- Quantification of Kcnq2 immunostaining intensity in olfactory epithelia of tdTomato$^{\Delta OMP}$ and IGF1R;tdTomato$^{\Delta OMP}$ mice (n=3 vs 3).

E,F,G- Heat, oxygen consumption and respiratory quotient of control and IGF1R$^{\Delta OMP}$ mice at the age of 15 weeks (n=11 vs 10).

H, I, J- Relative mRNA expression in iWAT, gWAT and BAT of control and IGF1R$^{\Delta OMP}$ mice at the age of 40 weeks (n=6 vs 6).

K- Glucose uptake in different tissues after a hyperinsulinemic-euglycemic CLAMP of control and IGF1R$^{\Delta OMP}$ mice at the age of 22 weeks (n=7 vs 8).

L- Serum levels of insulin, leptin and corticosterone in control and IGF1R$^{\Delta OMP}$ mice at the age of 40 weeks (n=6 vs 6).

***p<0.001, **p<0.001, *p<0.05, two-tailed unequal variance Student's *t* test unless specified. All values denote means ± SEM.

Fig. S1

A

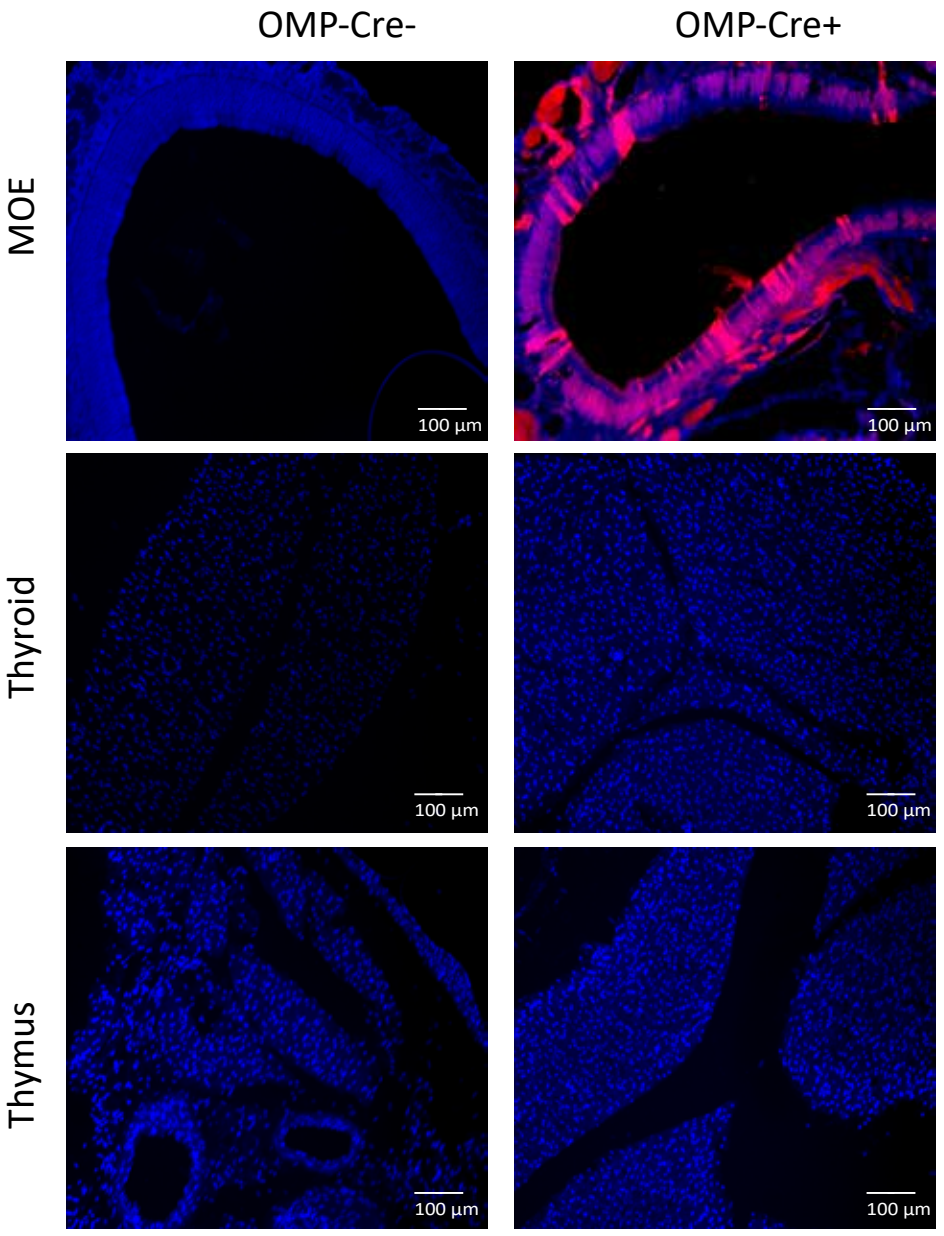
OMP-Cre-
OMP-Cre+
MOE
Thyroid
Thymus
100 µm

B

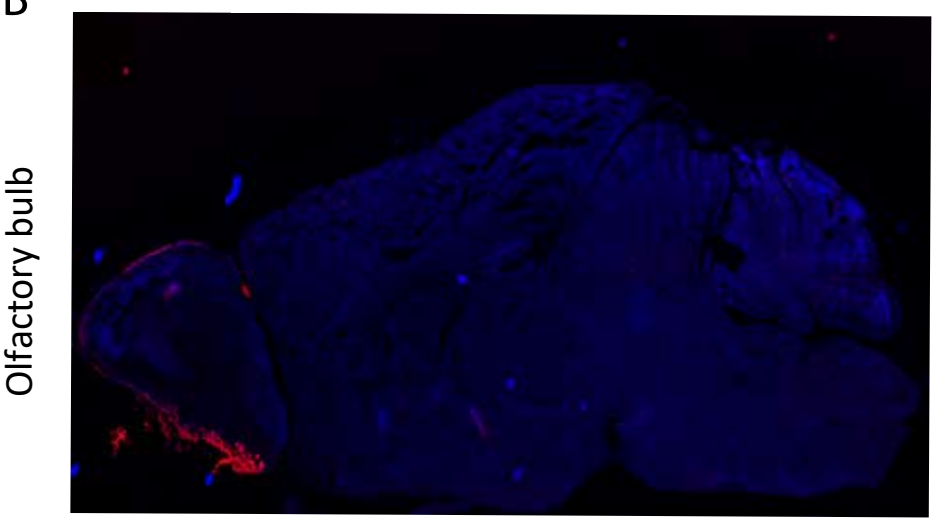
OMP-Cre+
Olfactory bulb

C

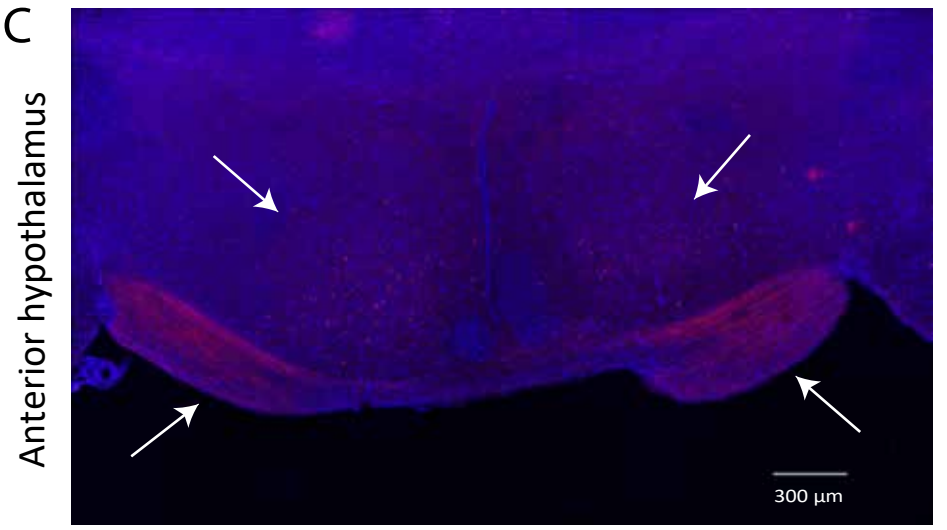
Anterior hypothalamus
300 µm

D

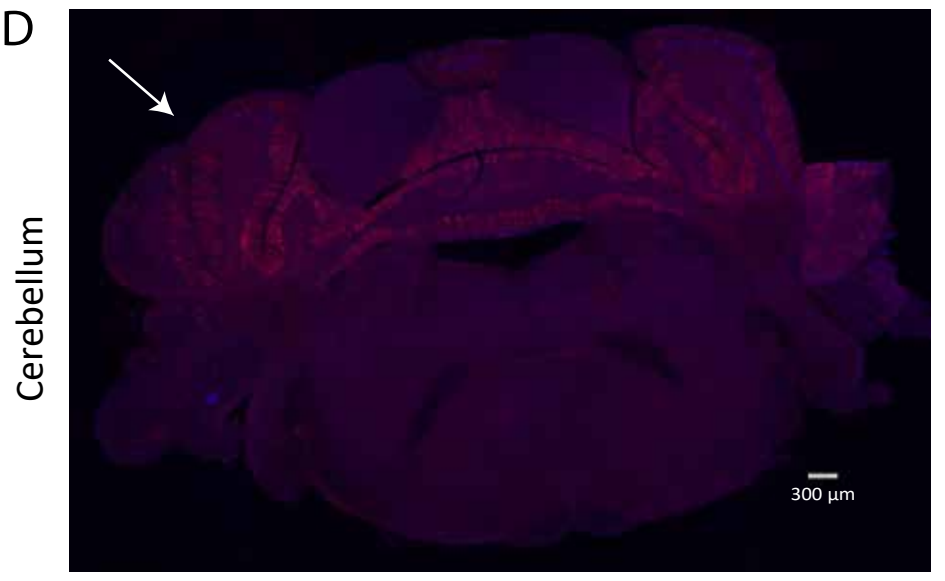
Cerebellum
300 µm

E

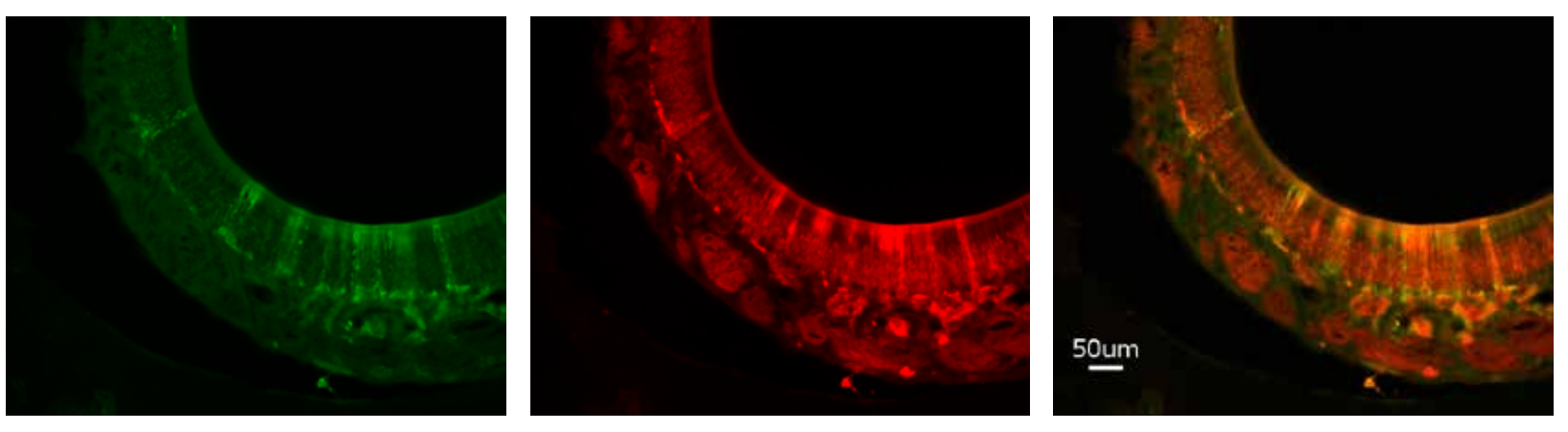
anti-dsRed
anti-OMP
overlay
MOE
50um

Fig. S2

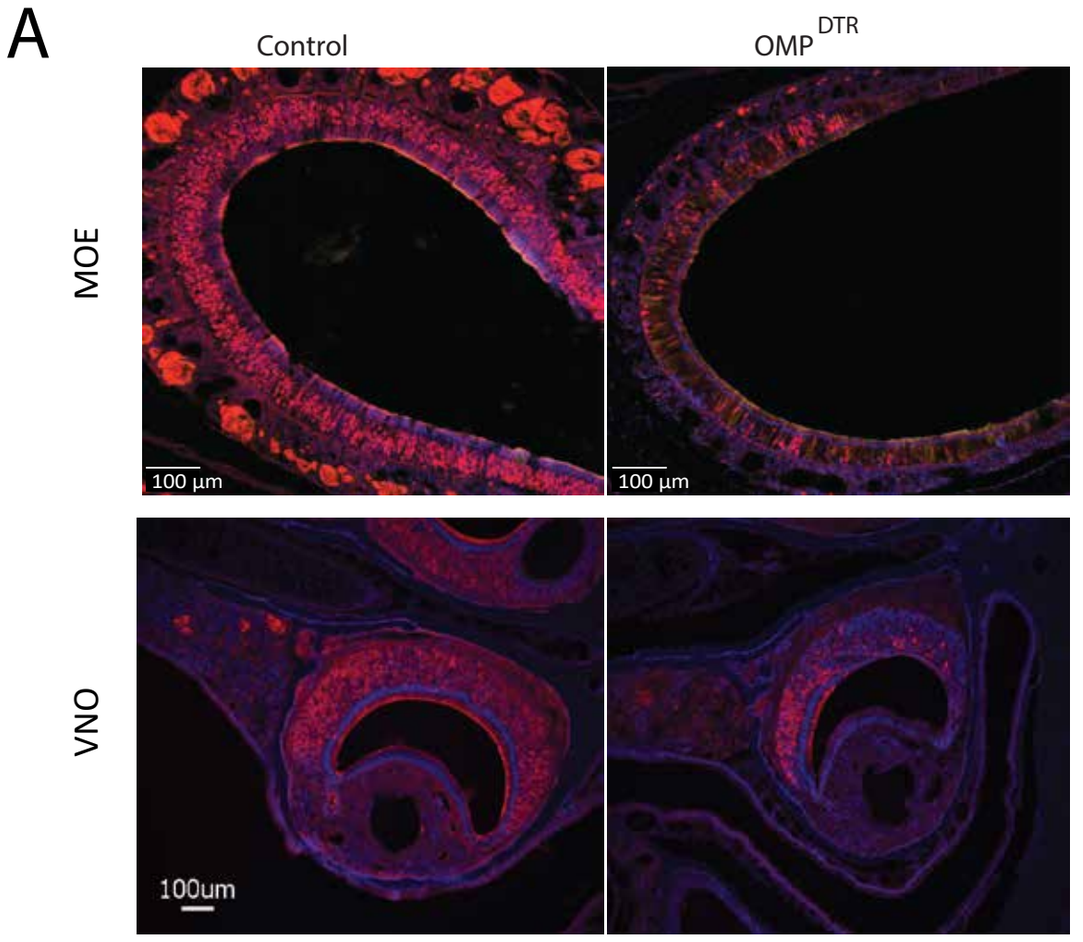
A
Control
OMP DTR
MOE
VNO
100 µm
100 µm
100um

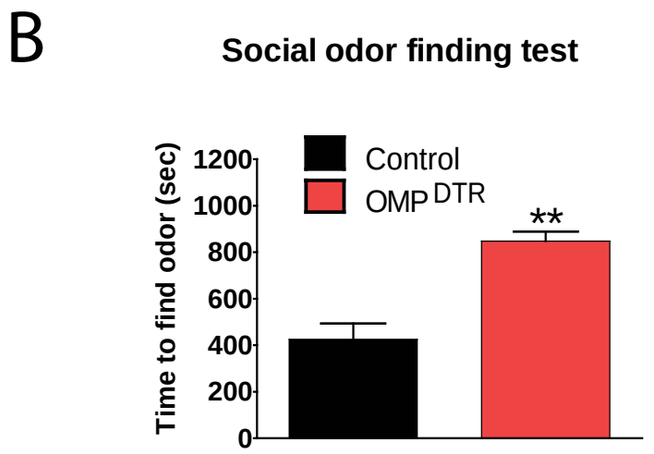
B
Social odor finding test
Time to find odor (sec)
1200
1000
800
600
400
200
0
Control
OMP DTR
**

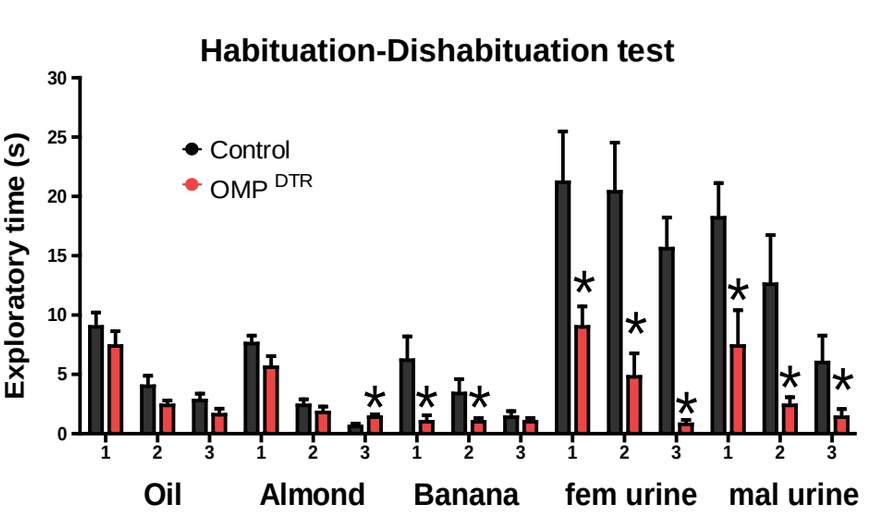
C
Habituation-Dishabituation test
Exploratory time (s)
30
25
20
15
10
5
0
Control
OMP DTR
1 2 3 1 2 3 1 2 3 1 2 3 1 2 3
Oil
Almond
Banana
fem urine
mal urine

Fig. S3

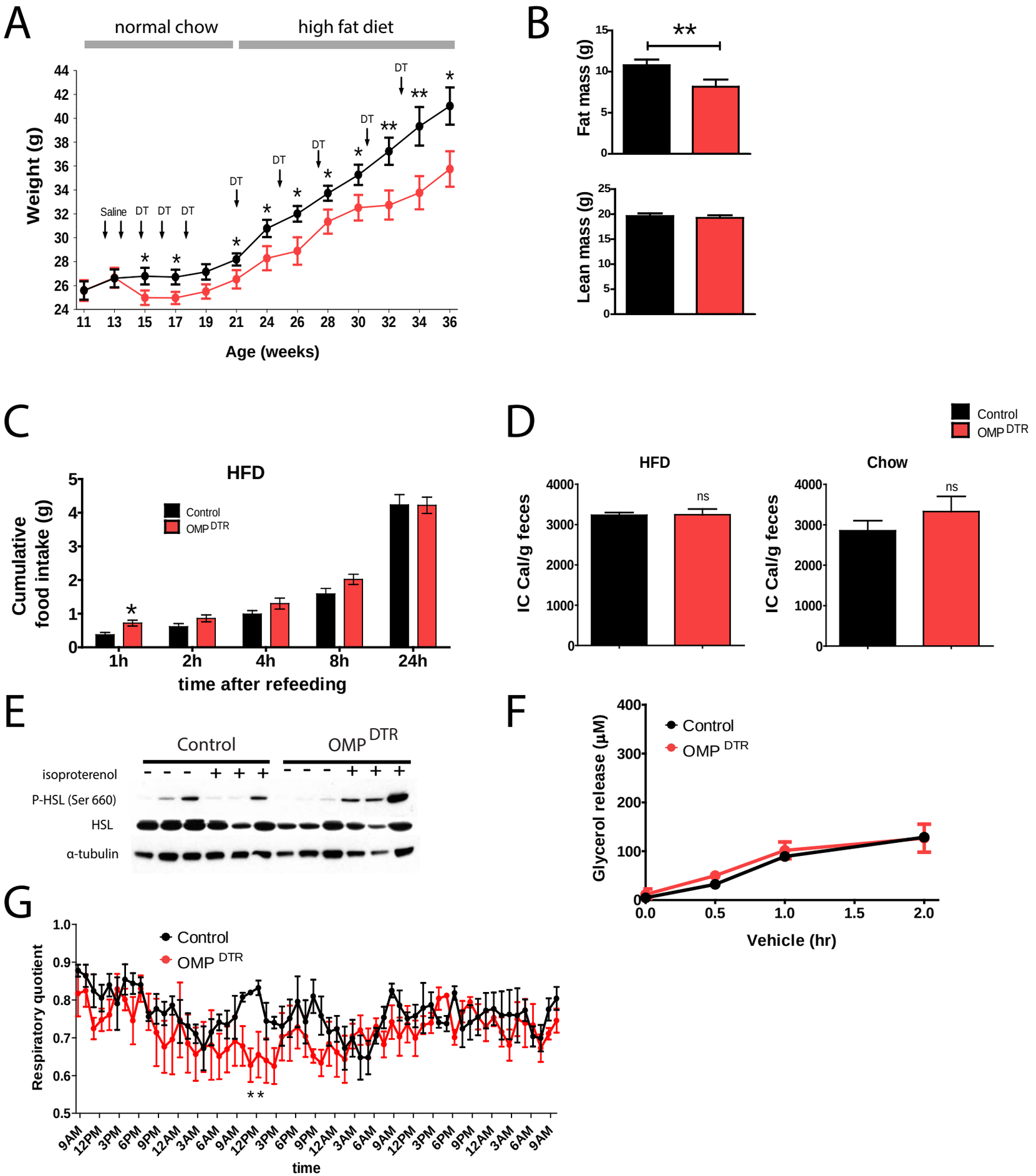
A
normal chow
high fat diet
Weight (g)
Age (weeks)
Saline
DT
B
Fat mass (g)
Lean mass (g)
**
C
HFD
Control
OMP DTR
Cumulative food intake (g)
time after refeeding
1h
2h
4h
8h
24h
D
HFD
Chow
IC Cal/g feces
ns
E
Control
OMP DTR
isoproterenol
P-HSL (Ser 660)
HSL
α-tubulin
F
Glycerol release (μM)
Vehicle (hr)
G
Respiratory quotient
time

Fig. S4

A

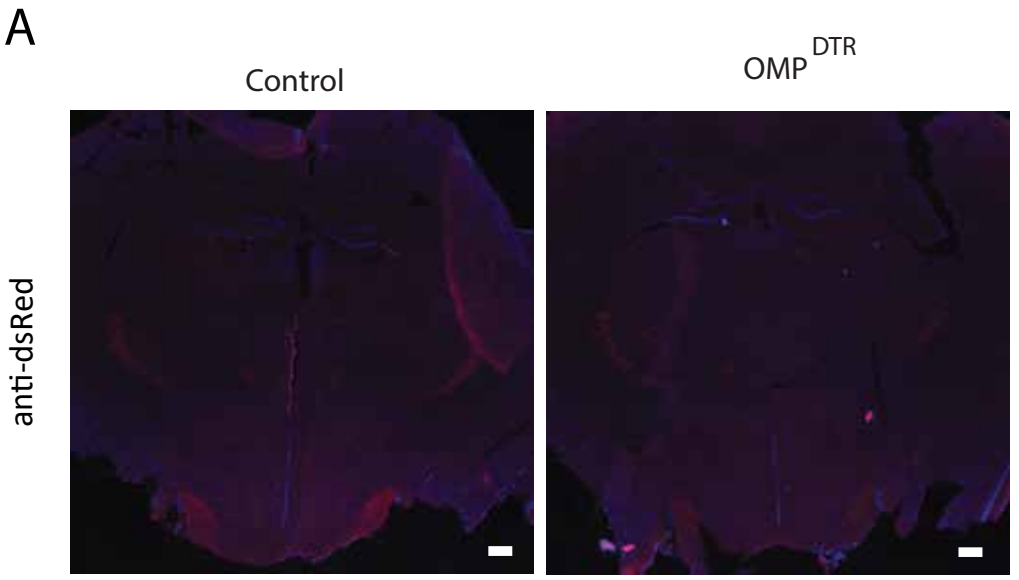

B

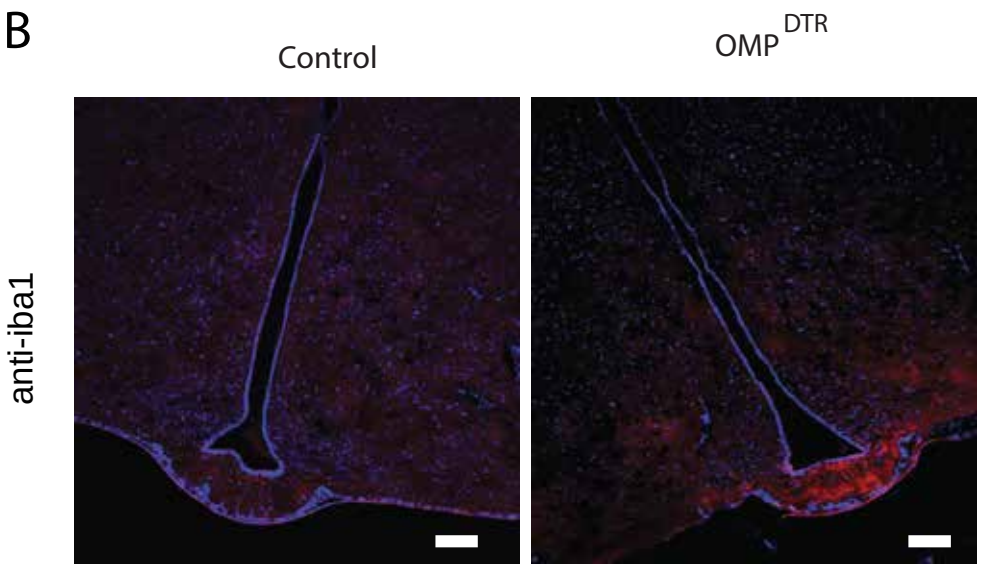

C

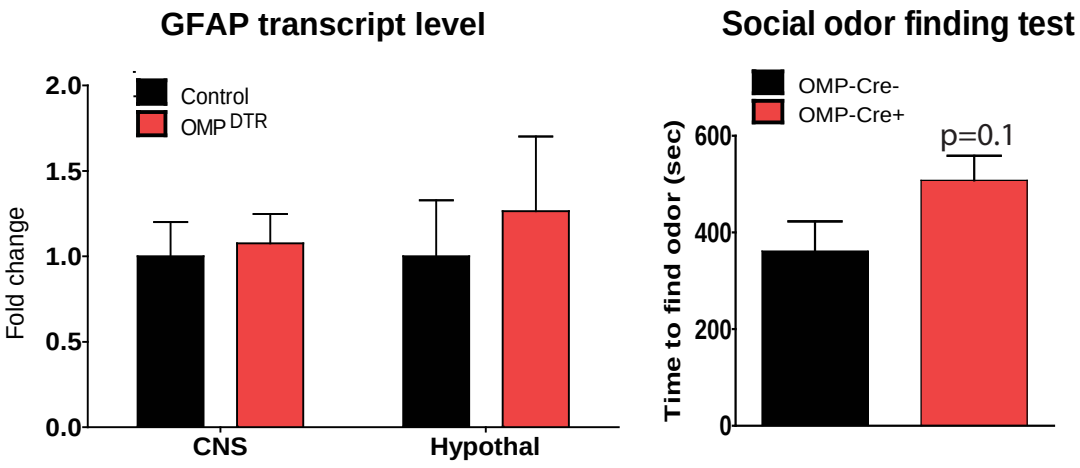

D

E

F

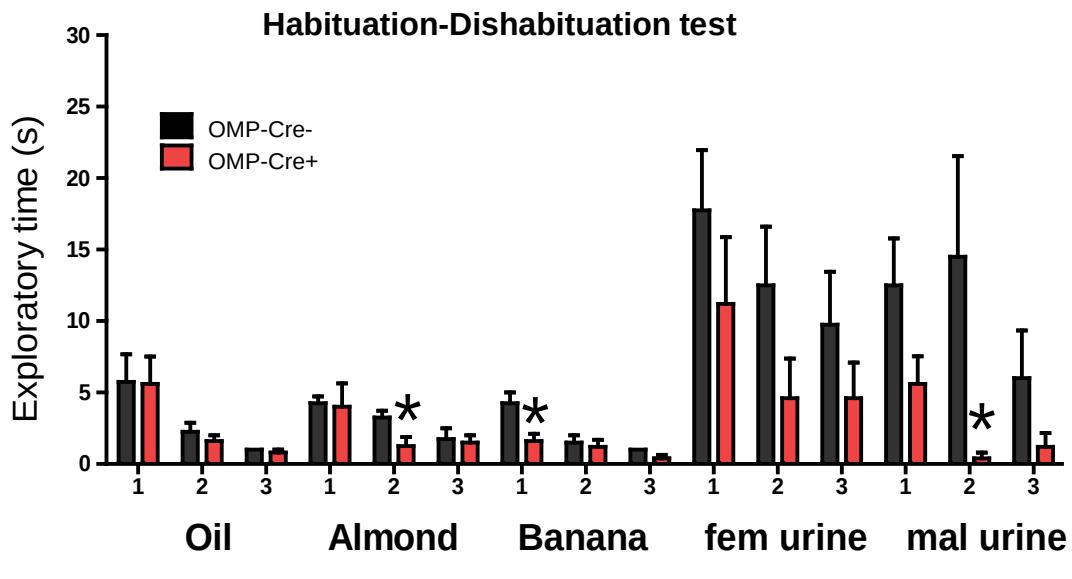

Fig. S5

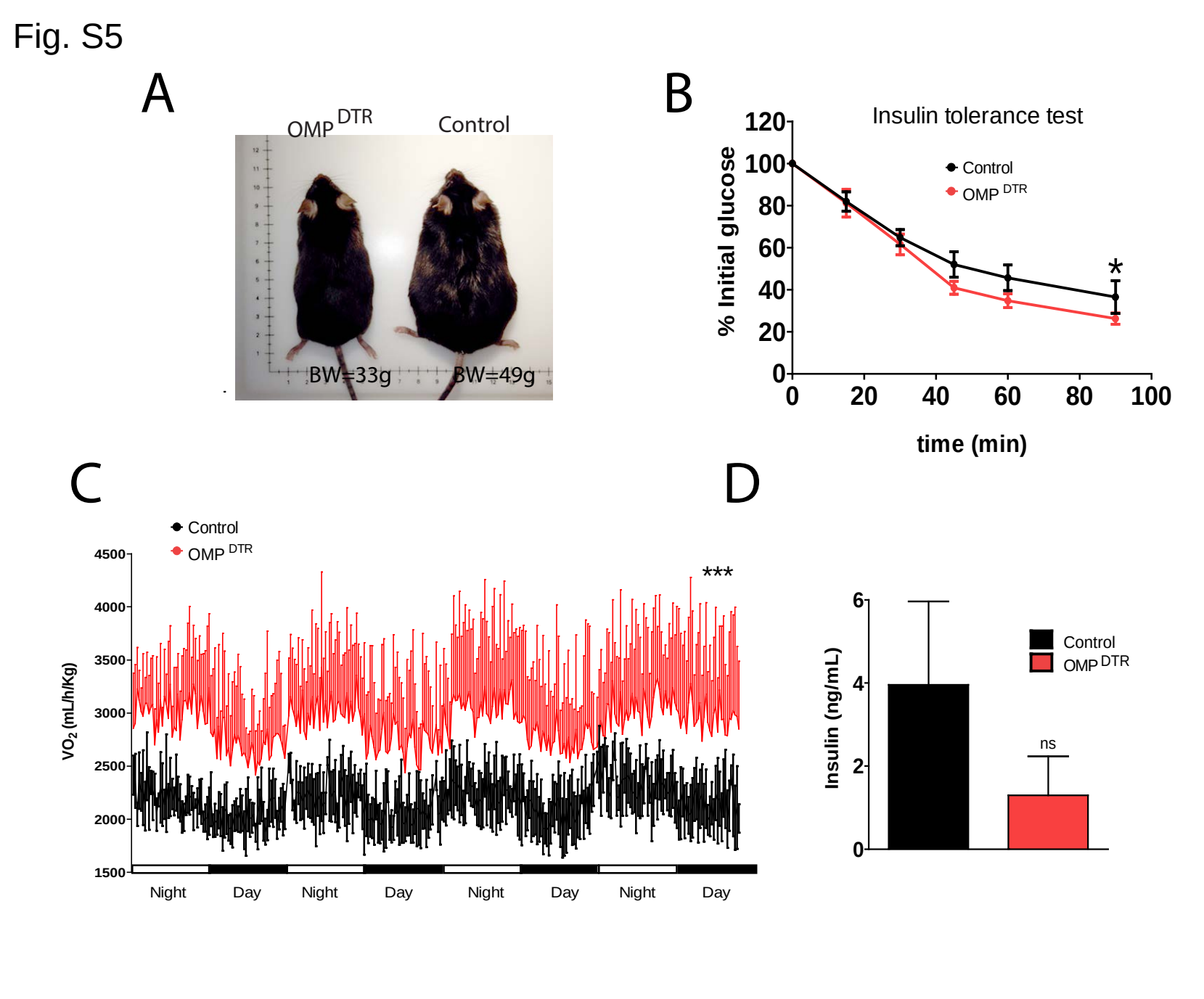
A
OMP DTR
Control
BW=33g
BW=49g
B
Insulin tolerance test
Control
OMP DTR
% Initial glucose
120
100
80
60
40
20
0
0
20
40
60
80
100
time (min)
*
C
Control
OMP DTR
4500
4000
3500
3000
2500
2000
1500
VO2 (mL/h/Kg)
***
Night
Day
Night
Day
Night
Day
Night
Day
D
Insulin (ng/mL)
6
4
2
0
Control
OMP DTR
ns

Fig. S6

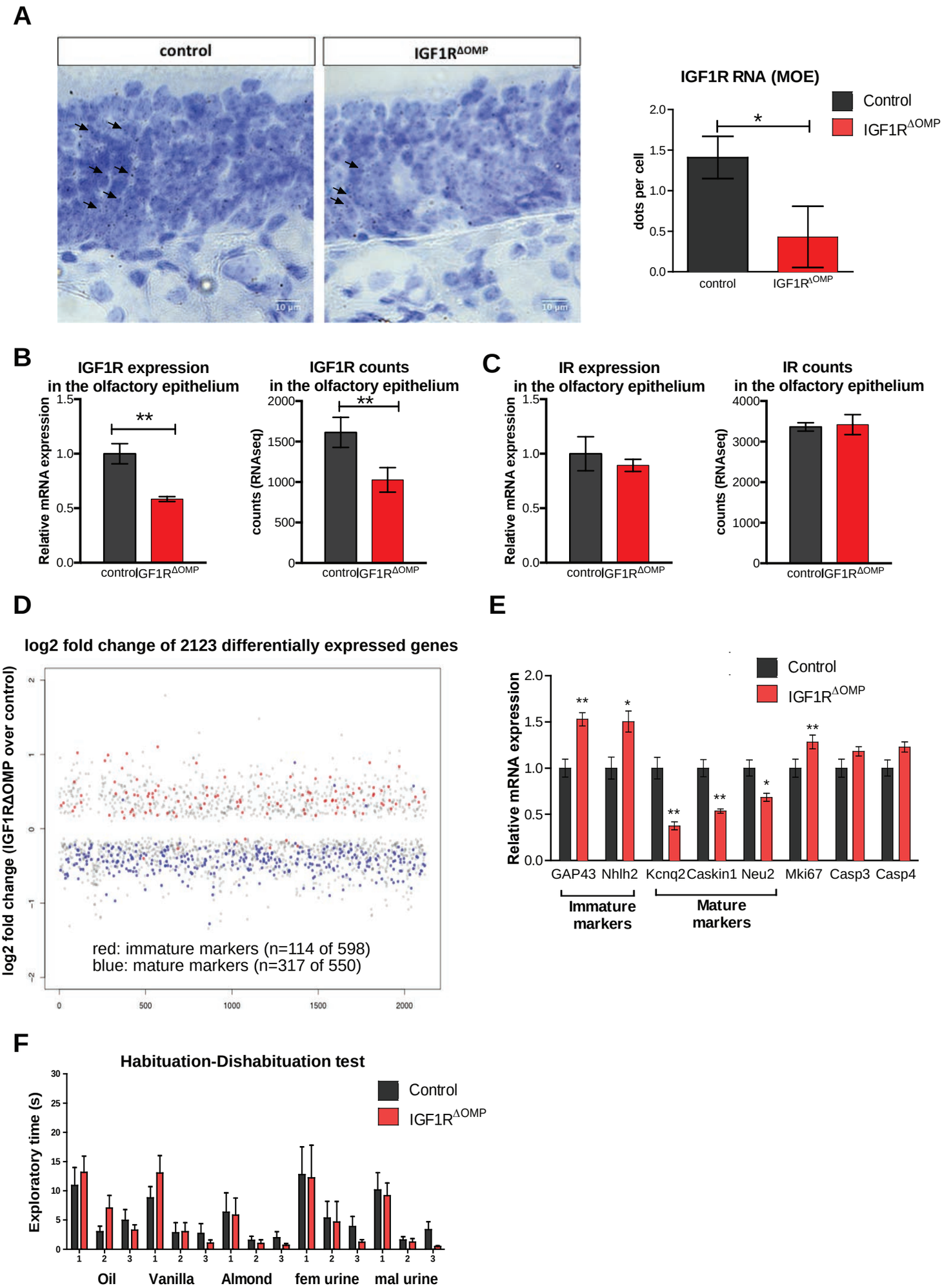
A
control
IGF1R^ΔOMP
10 µm
IGF1R RNA (MOE)
Control
IGF1R^ΔOMP
dots per cell
control
IGF1R^ΔOMP
B
IGF1R expression in the olfactory epithelium
Relative mRNA expression
IGF1R counts in the olfactory epithelium
counts (RNAseq)
C
IR expression in the olfactory epithelium
IR counts in the olfactory epithelium
D
log2 fold change of 2123 differentially expressed genes
log2 fold change (IGF1RΔOMP over control)
red: immature markers (n=114 of 598)
blue: mature markers (n=317 of 550)
E
Relative mRNA expression
GAP43
Nhlh2
Kcnq2
Caskin1
Neu2
Mki67
Casp3
Casp4
Immature markers
Mature markers
F
Habituation-Dishabituation test
Exploratory time (s)
Oil
Vanilla
Almond
fem urine
mal urine

Fig. S7

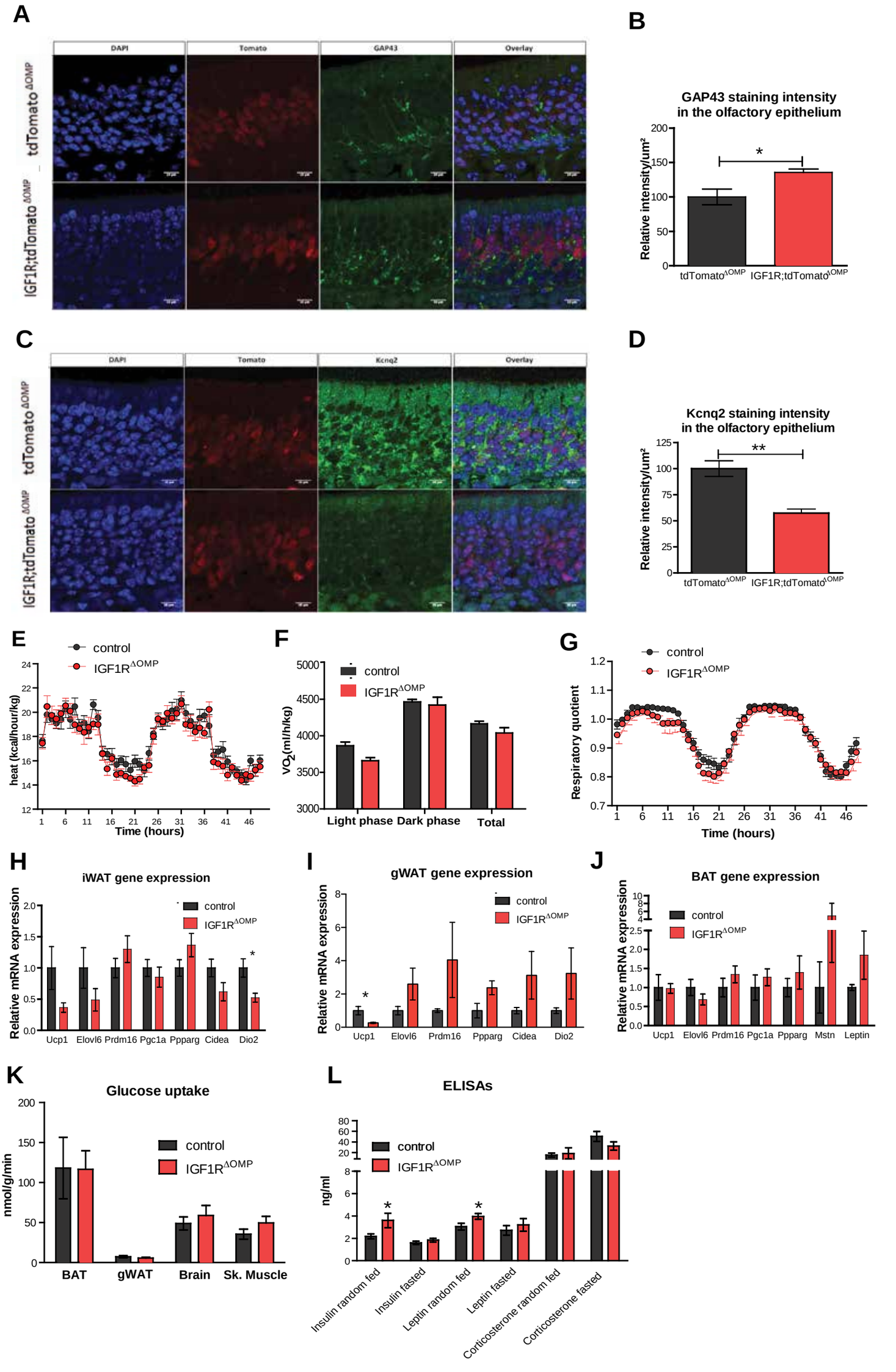
A
DAPI
Tomato
GAP43
Overlay
tdTomato ΔOMP
IGF1R;tdTomato ΔOMP
B
GAP43 staining intensity in the olfactory epithelium
Relative intensity/um²
tdTomato ΔOMP
IGF1R;tdTomato ΔOMP
C
DAPI
Tomato
Kcnq2
Overlay
D
Kcnq2 staining intensity in the olfactory epithelium
E
control
IGF1R ΔOMP
heat (kcal/hour/kg)
Time (hours)
F
VO2(ml/h/kg)
Light phase
Dark phase
Total
G
Respiratory quotient
Time (hours)
H
iWAT gene expression
Relative mRNA expression
Ucp1
Elovl6
Prdm16
Pgc1a
Ppparg
Cidea
Dio2
I
gWAT gene expression
J
BAT gene expression
Mstn
Leptin
K
Glucose uptake
nmol/g/min
BAT
gWAT
Brain
Sk. Muscle
L
ELISAs
ng/ml
Insulin random fed
Insulin fasted
Leptin random fed
Leptin fasted
Corticosterone random fed
Corticosterone fasted

Table S1. Primer sequences used for Quantitative PCR analysis, related to STAR Methods (Quantitative PCR analysis).

Transcript	Sequence	Specific use
18s	4308329 (Applied Biosystems)	
F β-actin	CTAAGGCCAACCGTGAAAAG	
R β-actin	ACCAGAGGCATACAGGGACA	
F ACAA1B	GAAAGCAGGGCTGACTGTGAAT	
R ACAA1B	GTAGACGGCCTGACTTGCAAA	
F acaa2	TTGATAGACGTGAACGAAGCTTTT	
R acaa2	GATCCAGGGCCTTCTGAACA	
F accbeta	TGCATGACGGAATTCTTGCA	
R accbeta	TCAATTCAACGTCCACAATGTTC	
F acox1	CAAGGCATGCACCATTGC	
R acox1	GCTCGCTTCTCTTGATTTCAGACT	
Fadiponectin	GCACTGGCAAGTTCTACTGCAA	
Radiponectin	GTAGGTGAAGAGAACGGCCTTGT	
F adrb3	GGCCCTCTCTAGTTCCCAG	
R adrb3	TAGCCATCAAACCTGTTGAGC	
F aP2	ACA CCG AGA TTT CCT TCA AAC TG	
R Ap2	CCA TCT AGG GTT ATG ATG CTC TTC A	
F bdnf	TCATACTTCGGTTGCATGAAGG	
R bdnf	AGACCTCTCGAACCTGCCC	
F ccl2	TTAAAAACCTGGATCGGAACCAA	
R ccl2	GCATTAGCTTCAGATTTACGGGT	
F ccl3	TTCTCTGTACCATGACACTCTGC	
R ccl3	CGTGGAATCTTCCGGCTGTAG	
F CD68	TTCTCCAGCTGTTCACCTTGACCT	
R CD68	GTTGCAAGAGAAACATGGCCCGAA	
F cidea	TGCTCTTCTGTATCGCCCAGT	
R cidea	GCCGTGTTAAGGAATCTGCTG	
F cpt1a	AAGTTCATCCGATTCAAGAATGG	
R cpt1a	TCACACCCACCACCACGAT	
F cpt1b	GACCCAAAACAGTATCCCAATCA	
R cpt1b	CGCCACGGGACCAAAG	
F cox4i1	ACCAAGCGAATGCTGGACAT	
R cox4i1	GGCGGAGAAGCCCTGAA	
Fcox5b	GCTGCATCTGTGAAGAGGACAAC	
Rcox5b	CAGCTTGTAATGGGTTCCACAGT	
F cox7a1	CAG CGT CAT GGT CAG TCT GT	
R cox7a1	AGA AAA CCG TGT GGC AGA GA	
F cox8b	GAA CCA TGA AGC CAA CGA CT	
R cox8b	GCG AAG TTC ACA GTG GTT CC	

F coxIII	GCAGGATTCTTCTGAGCGTTCT	
R coxIII	GTCAGCAGCCTCCTAGATCATGT	
F cyt-c	GCAAGCATAAGACTGGACCAAA	
R cyt-c	TTGTTGGCATCTGTGTAAGAGAATC	
F cxcl1	CTGGGATTCACCTCAAGAACATC	
R cxcl1	CAGGGTCAAGGCAAGCCTC	
F dio2	CAGTGTGGTTGCACGTCTCCAATC	
R dio2	TGAACCAAAGTTGACCACCAG	
F F4/80*	CCCCAGTGTCCTTACAGAGTG	
R F4/80*	GTGCCCAGAGTGGATGTCT	
gapdh	4308313 (Applied Biosystems)	
F MCAD	GCCAATGATGTGTGCTTACTGTGT	
R MCAD	ATGGCCGCCACATCAGA	
F MCD	GCACGTCCGGGAAATGAA	
R MCD	CGGAGGAGAACCACTCAGACA	
F LCAD	CTCAATGGAAGCAAGGTGTTCA	
R LCAD	GCCACGACGATCACGAGAT	
F ppar gamma	CACAAGAGCTGACCCAATGGT	
F ppar gamma	GATCGCACTTTGGTATTCTTGGA	
F pgc1α	CCCTGCCATTGTTAAGACC	
R pgc1α	TGCTGCTGTTCCTGTTTTC	
F ppar-γ	CACAAGAGCTGACCCAATGGT	
R ppar-γ	GATCGCACTTTGGTATTCTTGGA	
F prdm16	CAGCACGGTGAAGCCATTC	
R prdm16	GCGTGCATCCGCTTGTG	
F tlr2	GCAAACGCTGTTCTGCTCAG	
R tlr2	AGGCGTCTCCCTCTATTGTATT	
F tnfa	CCCTCACACTCAGATCATCTTCT	
R tnfa	GCTACGACGTGGGCTACAG	
F ucp1	ACTGCCACACCTCCAGTCATT	
R ucp1	CTTTGCCTCACTCAGGATTGG	
F ucp2	CGGTCCGGACACAATAGTATGA	
R ucp2	GCCCGATCCCCTCGATT	
F ucp3	AGATGGTGGCTCAGGAGGG	
R ucp3	CCCAGACGCAGAAAGGAGG	
Ucp1 (Taqman)	Mm00494069_m1	OMP ΔIGF1R
Elovl6 (Taqman)	Mm00851223_s1	OMP ΔIGF1R
Prdm16 (Taqman)	Mm00712556_m1	OMP ΔIGF1R
Pparg (Taqman)	Mm00440945_m1	OMP ΔIGF1R
Cidea (Taqman)	Mm00432554_m1	OMP ΔIGF1R
Dio2 (Taqman)	Mm00515664_m1	OMP ΔIGF1R
Ppargc1a (Taqman)	Mm00447183_m1	OMP ΔIGF1R
Lep (Taqman)	Mm00434759_m1	OMP ΔIGF1R

Mstn (Taqman)	Mm01254559_m1	
Gap43 (Taqman)	Mm00500404_m1	
Nhlh2 (Taqman)	Mm01959164_u1	
Omp (Taqman)	Mm00448081_s1	OMP ΔIGF1R
Caskin 1 (Taqman)	Mm01300046_m1	
Neu2 (Taqman)	Mm00479238_m1	
Kcnq2 (Taqman)	Mm00440080_m1	
Casp4 (Taqman)	Mm00432304_m1	
Mki67 (Taqman)	Mm01278617_m1	